Alternative splicing of a potato disease resistance gene maintains homeostasis between development and immunity, and functions as a novel process for pathogen surveillance

Biying Sun[1,2], Jie Huang[1,2], Chuyun Gao[1,2], Kangping Li[1], Fei Zhao[1], Liang Kong[1,2], Luyao Wang[1,5], Jiayong Shen[1], Yuanchao Wang[1,2], Dennis A. Halterman[3,4,*], Suomeng Dong[1,2,*]

[1]Department of Plant Pathology, Nanjing Agricultural University, Nanjing 210095, China.

[2]The Key Laboratory of Integrated Management of Crop Diseases and Pests (Ministry of Education), Nanjing Agricultural University, Nanjing 210095, China.

[3]Department of Plant Pathology, University of Wisconsin-Madison, Madison, Wisconsin, United States of America.

[4]U.S. Department of Agriculture-Agricultural Research Service, Vegetable Crops Research Unit, Madison, Wisconsin, United States of America

[5]Shenzhen Branch, Guangdong Laboratory of Lingnan Modern Agriculture, Genome Analysis Laboratory of the Ministry of Agriculture and Rural Affairs, Agricultural Genomics Institute at Shenzhen, Chinese Academy of Agricultural Sciences, Shenzhen, Guangdong, 518120, China.

*Address correspondence to: smdong@njau.edu.cn, dennis.halterman@usda.gov

Short title:

Resistance gene alternative splicing regulates development and immunity homeostasis

One-sentence summary:

Potato resistance gene *RB* balances plant growth and immunity through AS, while pathogen-secreted effector IPI-O1 mediates AS of *RB* by targeting the conserved splicing factor StCWC15, further increasing the *RB_CDS* expression level to activate immunity.

Abstract

Plants possess a robust and sophisticated innate immune system against pathogens. The intracellularly localized receptors with nucleotide-binding, leucine-rich repeat (NLR) motifs recognize pathogen-derived effector proteins to trigger the immune response. To balance plant growth with rapid pathogen detection, NLR expression is precisely controlled in multifaceted ways. The role of post-transcriptional processing of NLRs, including alternative splicing (AS) of introns, in response to infection is an important area of research that requires further study. Here we report that the potato NLR gene *RB* undergoes AS of its intron, resulting in two transcriptional isoforms, which coordinately regulate plant immunity and growth homeostasis. *RB* mainly exists as intron-retained isoform *RB_IR* encoding a truncated lost-function RB protein to maintain plant normal growth without pathogen infection. Upon late blight infection, the causal pathogen *Phytophthora infestans* induces intron splicing of *RB*, increasing the abundance of *RB_CDS*, which encodes a full-length, and active R protein. By deploying the *RB* splicing isoforms fused with *luciferase* reporter system, we identified IPI-O1 (also known as Avrblb1), the RB cognate effector, as a facilitator of *RB* AS. Importantly, IPI-O1 directly interacts with potato splicing factor StCWC15 to promote *RB* splicing for activation of *RB*-mediated resistance. Thus, our study reveals that StCWC15 serves as a surveillance facilitator sensing the pathogen-secreted effector maintaining the trade-off between *RB*-mediated plant immunity and growth, expanding our understanding of molecular plant-microbe interactions.

Keywords: potato late blight; resistance gene; RB; IPI-O1; CWC15

Introduction

Upon pathogen infection, plants have evolved two major mechanisms for recognition of pathogen effectors and elicitation of plant defense (Jones and Dangl, 2006). One utilizes plasma membrane-localized pattern-recognition receptors (PRRs) to perceive pathogen-associated molecular patterns (PAMPs), leading to PAMP-triggered immunity (PTI) (Couto and Zipfel, 2016). The other uses intracellular NLR immune receptors to detect cytoplasmic effectors introduced by the pathogen, thereby activating effector-triggered

immunity (ETI; Jones and Dangl, 2006; Dodds and Rathjen, 2010; Cui et al., 2015). During ETI, NLRs oligomerize to form "resistosome" structures (Wang et al., 2019; Ofir et al., 2021) and the response culminates in programmed cell death, known as the hypersensitive response (HR), to prevent pathogen spread. The enormous diversity of *NLR* genes in plants demonstrates their important role in plant immunity (Li et al., 2015; Van de Weyer et al., 2019).

Late blight, caused by oomycete *Phytophthora infestans*, is the most devastating disease in potato production (Haverkort et al., 2009; Kamoun et al., 2015; Sun et al., 2022). Deployment of host resistance (R) genes is a crucial strategy for controlling the disease and many potato cultivars have been bred to introduce resistance genes against *P. infestans* (*Rpi* genes) that originate from potato wild relatives (Kamoun and Smart, 2005; Karki et al., 2021). More than 70 *Rpi* genes have been identified and mapped in 32 *Solanum* species (Paluchowska et al., 2022). Among these *R* genes, *RB* was cloned from the wild diploid potato species *Solanum bulbocastanum*, and is known for its durable late blight resistance (Song et al., 2003; van der Vossen et al., 2003). Like most plant *R* genes, *RB* encodes an NLR protein. It recognizes *P. infestans* effector IPI-O1 (also known as Avrblb1) to activate immune responses (Vleeshouwers et al., 2008; Champouret et al., 2009). Previous research has demonstrated that IPI-O1 could be recognized by RB and hypothesized that IPI-O1 changes the conformation of RB to facilitate the formation a functional multimeric complex, thereby activating *RB*-mediated disease resistance (Chen et al., 2012; Zhao and Song, 2021).

Despite their usefulness in activating resistance, constitutive expression of *NLR* genes causes auto-immunity, leading to a negative effect on plant growth and development (Cheng et al., 2011; Deng et al., 2019; Cui et al., 2020). Therefore, the expression of *NLR* genes needs to be precisely regulated to maintain homeostasis between growth and immunity. The regulation mechanisms for the expression of NLRs are mainly via transcription regulation, RNA processing, post-translational modification and proteasome-mediated degradation (Li et al., 2015). Intron splicing is common in post-transcriptional RNA processing and is executed by a supramolecular ribonucleoprotein (RNP) complex known as the spliceosome (Reddy, 2007). Intron retention during RNA processing is a form of alternative splicing (AS) and can lead to changes in the translated protein. AS contributes to transcriptome and proteome

diversity in animals and plants and it has been shown to play an important role in regulating plant immunity (Reddy et al., 2013b; Wu et al., 2016; Bazin et al., 2020; Zhang et al., 2022). Several *NLR* genes have been demonstrated to undergo AS, suggesting that this may be an important mechanism for regulation of this important class of immunity-related genes (Dinesh-Kumar and Baker, 2000; Halterman et al., 2003; Halterman and Wise, 2006; Sanchez-Martin et al., 2021). The splicing regulation of NLR had been reported (Xu et al., 2012). However, the molecular mechanisms that control *NLR* gene AS and the significance of AS in maintaining plant growth and immunity homeostasis is incompletely understood.

In this work, we report that the potato resistance gene *RB* undergoes alternative splicing, resulting in generation of two transcripts. Removal of the intron results in intact RB protein that confers resistance to *P. infestans*, while intron retention results in a truncated RB protein that cannot protect against the pathogen. Upon late blight infection, *P. infestans* is able to modulate the AS of *RB*, increasing the abundance of *RB_CDS* to activate *RB*-mediated immunity. Interaction of *P. infestans* effector IPI-O1 with splicing factor CWC15 in the nucleus leads to an increase of *RB* intron splicing during infection. This process balances plant growth and defense and provides a unique molecular basis for NLR recognition of pathogen effectors.

Results

P. infestans promotes *RB* intron splicing

The *RB* gene contains a single 679nt intron beginning 428nt downstream of the translation start codon (Figure 1A). To investigate AS of the *RB* intron, we performed rapid amplification of cDNA ends (5' RACE) using RNA from non-inoculated *RB* transgenic potato cv. Katahdin expressing a single genomic copy of *RB* with its native promoter (SP951; Bradeen et al., 2009). Two transcriptional isoforms were identified that correspond to the transcripts with the intron spliced (*RB_CDS*) or retained (*RB-IR*) (Fig. 1A and Supplemental Fig. S1). We further examined AS of *RB* in SP951 and *RB* transgenic *Nicotiana benthamiana* by reverse transcription PCR (RT-PCR). We identified two transcripts corresponding to *RB_CDS* and *RB_IR* in plants with *RB*, but no transcripts in non-transgenic controls (Fig. 1B). Splicing of introns in pre-mRNA is directed by spliceosome targeting of particular sequences

117 at the intron/exon junctions called splice sites (Wan et al., 2020) and are commonly found
118 with a conserved GT dinucleotide at the 5' splice site and a conserved AG dinucleotide at the
119 3' splice site (Sheth et al., 2006). We synonymously mutate the splice sites in *RB* from GT to
120 GA (5') and from AG to CG (3') resulted in the inability of transiently expressed *RB_IVS*
121 (IVS=intervening sequence) to undergo intron splicing in both potato and *N. benthamiana*
122 (Fig. 1B). Among the two transcripts of *RB*, *RB_CDS* encodes the entire NLR protein, while
123 *RB_IR* encodes a truncated protein containing only the CC domain, due to a premature
124 termination codon (PTC) in the intron (Fig. 1C). Immunoblot analysis revealed that the
125 translation products from both RB_CDS and RB_IR with Myc tags can be detected (Fig. 1D).
126 To investigate the dynamic change of *RB* splicing during pathogen infection, we
127 inoculated *RB* transgenic potato SP951 with *P. infestans* isolate JH19 and measured the
128 transcript levels of different isoforms of *RB* compared to levels following water (mock)
129 inoculation. The results show that the relative expression intensity of the *RB_IR* isoform was
130 reduced at 1 and 2 dpi, whereas the relative expression intensity of the *RB_CDS* isoform
131 increased during the same timeframe (Fig. 2A). We also inoculated SP951 with zoospores of
132 *Phytophthora capsici* isolate LT1534 and monitored the level of transcripts compared to
133 mock. We found that *P. capsici* had no effect on the relative expression of either *RB* transcript
134 (Fig. 2A). Quantitative RT-PCR data demonstrated that the splicing ratio (transcript level of
135 the spliced isoform divided by the transcript level of the unspliced isoform) of *RB*
136 *(RB_CDS/RB_IR)* significantly increased to 1.66 at 1 dpi and 2.78 at 2 dpi following JH19
137 inoculation, indicating an increase in *RB_CDS* expression and a decrease of *RB_IR*
138 expression during *P. infestans* infection (Fig. 2B and Supplemental Fig. S2A). *RB* splicing
139 ratios remained unchanged in *P. capsici* inoculated plants and mock treatment (Fig. 2B and
140 Supplemental Fig. S2A). Following these experiments, we found the total gene expression of
141 *RB* did not change significantly in either *P. infestans*-, *P. capsici-,* or mock-inoculated plants
142 (Supplemental Fig. S2B). Together, these results indicate that the *RB* gene produces more
143 *RB_CDS* transcript due to increased intron splicing following inoculation of *P. infestans*.
144
145 **Intron splicing of *RB* is necessary for the activation of resistance and functions**
146 **independent of ETI**

147 To test whether intron splicing can impact the ability of *RB* to confer *P. infestans*
148 resistance, we stably transformed wild-type *RB*, *RB_CDS*, *RB_IR*, and *RB_IVS* into potato
149 cultivar Favorita. We found the multiple potato plants expressing the wild-type *RB* and
150 *RB_CDS* exhibited clear resistance to *P. infestans*, while plants expressing *RB_IR* or *RB_IVS*
151 showed severe disease symptoms (Fig. 3A). The results of detached leaf assays of the
152 transgenic potatoes were consistent with the whole plant phenotypes (Fig. 3B). We also
153 created *RB*, *RB_CDS*, *RB_IR*, and *RB_IVS* transgenic *N. benthamiana* for our assays, and
154 found that *RB* and *RB_CDS* limited *P. infestans* lesion development and induced an HR
155 following expression of the *RB*-corresponding effector IPI-O1, while *RB_IR* and *RB_IVS* did
156 not (Supplemental Fig. S3).

157 The splicing process is executed by the spliceosome, which is conserved in eukaryotes
158 and is dynamically composed of a ribonucleoprotein complex (Chen and Manley, 2009). We
159 further tested whether AS of *RB* and immunity activation induced by *P. infestans* is affected
160 following silencing of spliceosome core components. We silenced orthologs of *U1-70k* (Chen
161 et al., 2020) and *SF3B1* (Finci et al., 2018) in *N. benthamiana* to test the effect on activation
162 of resistance mediated by intron-containing NLR and intron-lacking NLRs. Following
163 silencing of *U1-70k* and *SF3B1*, co-infiltration of the intron-containing *NLR* genes *RB* or
164 *Rpi-blb2* with the corresponding effectors *IPI-O1* and *Avrblb2*, respectively, elicited a
165 significantly weakened HR (Supplemental Fig. S4, A-C). However, co-infiltration of the
166 intronless NLRs *RB_CDS* or *R3a* with the corresponding effectors *IPI-O1* and *Avr3a*,
167 respectively, induced a strong HR following silencing of *U1-70k* and *SF3B1* (Supplemental
168 Fig. S4, A-C). We also silenced the RNA-binding protein *GRP7*, which is reported to regulate
169 RNA processing to affect the PTI response and specifically affect NLR protein Gpa2/Rx1
170 mediated immunity (Wang et al., 2020; Sukarta et al., 2022). *GRP7* silencing had no effect on
171 suppression of the HR following co-infiltration of any tested NLRs with their corresponding
172 effectors (Supplemental Fig. S4, A-C). We further silenced *U1-70k, SF3B1*, and *GRP7* in *RB*
173 transgenic *N. benthamiana* to test their effect on *RB*-mediated resistance to *P. infestans*. The
174 results show that silencing of *U1-70k* and *SFB1* rendered *RB* transgenic *N. benthamiana*
175 susceptible to *P. infestans* compared to the EV control (Fig. 4, A and B). However, it was
176 observed that the silencing of *GRP7* did not have a significant effect on *RB*-mediated

177 resistance (Fig. 4, A and B). Previously, we have observed that the *RB_CDS* transcript
178 isoform was most prevalent following *P. infestans* infection. We therefore tested the effect of
179 *U1-70k, SF3B1*, and *GRP7* on *RB* AS. The quantitative PCR results indicated that silencing
180 of *U1-70k* and *SF3B1* both significantly suppressed *RB* splicing ratio up-regulation following
181 *P. infestans* inoculation compared to the water-inoculated control (Fig. 4C and Supplemental
182 Fig. S4D). Consistent with our previous results, silencing of *GRP7* did not affect the
183 induction of *RB* splicing following infection (Fig. 4C and Supplemental Fig. S4D). To further
184 validate the role of the intron splicing in *RB* function, we conducted a chemical splicing
185 inhibitor assay. The splicing modulator Pladienolide B (Pla-B), interferes with splicing by
186 targeting SF3B1 and inhibiting its proper recognition with the intron (Kotake et al., 2007;
187 Cretu et al., 2018). We found that treatment with 30 μM Pla-B significantly reduced the
188 incidence of HR following co-infiltration with *RB*/*IPI-O1*, but did not affect HR incidence
189 following *RB_CDS*/*IPI-O1* co-infiltration (Fig. 4D). Furthermore, we examined splicing ratio
190 changes of *RB* induced by *P. infestans* following Pla-B treatment. The transcript-expression
191 analysis indicates 30μM Pla-B repressed the splicing ratio increase during infection (Fig. 4E
192 and Supplemental Fig. S4E). These results suggest that *P. infestans* modulates *RB* pre-mRNA
193 AS changes to initiate *RB* immune responses.
194
195 **IPI-O1 mediates *RB* splicing during the infection process**
196 To determine the specific protein secreted by *P. infestans* to regulate *RB* intron splicing,
197 we designed an *RB* alternative splicing reporter system that can directly reflect the extent of
198 *RB* intron splicing. The *RB* AS reporter system can detect the modulation of intron splicing
199 without ETI activation. The reporter is made up of the AS region of *RB* genomic sequences
200 (from 1 nt to 1987 nt) fused with the luciferase (*LUC*) reporter gene downstream of the intron
201 splicing site. The *RB-LUC* reporter system is predicted to produce two transcripts (Fig. 5A):
202 the first is *RB_IR-LUC*, which retains the intron, introduces a premature termination codon,
203 and does not produce a LUC signal; the second is *RB_CDS-LUC*, in which the intron is
204 spliced and translates a complete RB CC-NB protein and functional LUC protein. To further
205 verify the intron splicing changes via the *RB* AS reporter system following *P. infestans*
206 inoculation, we transiently expressed *RB-LUC* using agrobacterium in *N. benthamiana* and

207 inoculated with *P. infestans* JH19. Luciferase activity was measured at 1 dpi and
208 demonstrated a significant increase of LUC activity produced by *RB-LUC* compared to the
209 mock (water-inoculated), whereas the LUC activity of *RB_CDS-LUC* and *LUC* control
210 constructs did not change following *P. infestans* inoculation (Supplemental Fig. S5). Taken
211 together, we verified the modulation of *P. infestans* on promoting *RB* intron splicing by the
212 *RB* AS reporter system, demonstrating the feasibility of this system. This supported using the
213 *RB* AS reporter system to screen for *P. infestans* effectors that promote RB splicing. Indeed,
214 we previously identified several splicing regulatory effectors (SRE) using another splicing
215 reporter system (Huang et al., 2020). To determine whether these SRE proteins specifically
216 modulate *RB* splicing, we co-expressed several SRE proteins with the *RB-LUC* reporter
217 system in *N. benthamiana*. Screening results show that only IPI-O1 (SRE8) significantly
218 induced *RB* intron splicing compared to the mock-infiltrated control (Fig 5B). Infiltration of
219 SRE proteins with *RB_CDS-LUC*, which lacks the intron, did not affect LUC activity (Fig. 5,
220 B and C). To further verify the relationship between SRE proteins regulating *RB* AS and
221 activation of *RB* resistance, we overexpressed SRE proteins in *RB*-transgenic *N. benthamiana*
222 leaves to observe *RB* splicing changes and HR elicitation. Consistent with screening results
223 on the *RB* AS reporter system, overexpression of IPI-O1 induced *RB* intron splicing and
224 elicitation of the HR, while overexpression of other SRE proteins had no effect on either
225 response (Supplemental Fig. S6). Overall, these data suggest that IPI-O1, the corresponding
226 effector of *RB*, promotes AS of the *RB* gene.

227

228 **Nuclear localization of IPI-O1 is required for RB-induced immune response**

229 IPI-O1 has been reported as a nuclear-localized effector protein (Wang et al., 2018), and
230 we further predicted the presence of a nuclear localization signal (NLS) motif within the
231 protein. Given that IPI-O1 can affect *RB* splicing and that it is localized to the nucleus, we
232 tested whether subcellular localization of IPI-O1 is correlated with its ability to affect *RB*
233 splicing and HR-elicitation activity. We generated an IPI-O1 mutant, IPI-O1^{nls}, in which a
234 total of seven key NLS motif amino acids K (lysine) and R (arginine) were mutated to A
235 (alanine), and monitored the subcellular localization of proteins by confocal microscopy (Fig.

236 6A). We found that IPI-O1^{nls} fails to accumulate in the nucleoplasm and nucleolus like
237 IPI-O1, and instead is localized primarily in the cytoplasm (Fig. 6, B-D). Next, we tested the
238 ability of IPI-O1^{nls} to induce the HR. The results showed that IPI-O1 induced the HR in both
239 *RB* and *RB_CDS* transgenic *N. benthamiana*, but not in *RB_IR* plants (Fig. 6E). The IPI-O1^{nls}
240 mutant failed to induce the HR in *RB N. benthamiana*, but was still able to elicit the HR in
241 *RB_CDS* transgenic *N. benthamiana* (Fig. 6E). We then examined IPI-O1 and IPI-O1^{nls}
242 function on the modulation of *RB* intron splicing and found that the *RB_CDS*/*RB_IR* splicing
243 ratio increased during overexpression of IPI-O1 but not IPI-O1^{nls} (Fig. 6F). Together, these
244 data suggest that *RB* intron splicing and immunity activation requires nuclear localization of
245 IPI-O1. Consistent with the splicing ratio analysis by RT-qPCR (Fig. 6F), the *RB-LUC*
246 reporter system verified that IPI-O1, but not IPI-O1^{nls}, significantly promoted *RB* splicing
247 (Fig. 6G). In conclusion, the nuclear localization of IPI-O1 has an effect on promoting *RB*
248 intron splicing and immunity activation, but it has no impact on the function of the
249 intron-spliced *RB_CDS*.
250

251 **IPI-O1 interacts physically with splicing factor CWC15 in the nucleus**

252 To identify the potential splicing regulators of *RB*, we performed an ULTImate
253 (Hybrigenics) yeast-two hybrid (Y2H) screen to identify IPI-O1-interacting proteins within a
254 *N. benthamiana* cDNA library. A total of 81.6 million interactions were analyzed and 254
255 clones were processed by sequencing of the prey inserts. Of these 254 clones, 28 contained
256 an insert with homology to the *CWC15* gene from *N. tomentosiformis* (LOC104090615).
257 CWC15 is a core component of the Nineteen complex within the spliceosome (Will and
258 Lührmann, 2011). We identified two *CWC15*-related gene sequences in the
259 double-monoploid potato DM-1-3: *Soltu.DM.10G000900.1* (*StCWC15a*) and
260 *Soltu.DM.07G027590.1* (*StCWC15b*), which encoded 231 aa (amino acid) and 228 aa
261 proteins respectively. StCWC15a and StCWC15b share 93% similarity at the amino acid
262 levels (Supplemental Fig. S7A). Y2H assays also verified the interaction of full-length
263 NbCWC15a and NbCWC15b with IPI-O1 (Fig. 7A). Analysis of CWC15 sequence variation
264 in multiple wild and cultivated potatoes determined that CWC15 is well conserved but

265 polymorphisms are detected (Supplemental Fig. S7B).

266 To further explore the interaction between IPI-O1 and mutant IPI-O1^{nls} with CWC15a/b
267 in potato, we performed co-immunoprecipitation *in planta*. The results showed that both
268 StCWC15a and StCWC15b interacted with IPI-O1, but the nuclear localization mutant
269 IPI-O1^{nls} did not interact with either protein (Fig. 7B). No interaction was observed between
270 StCWC15 proteins and *P. infestans* effector Pi04314, another RxLR effector that interacts
271 with three host protein phosphatase 1 catalytic isoforms, causing their re-localization from
272 the nucleolus to the nucleoplasm (Boevink et al., 2016). The interactions were verified *in*
273 *vitro* by GST-pull down and Y2H, and were consistent with the co-IP assay (Fig. 7, C and D).
274 These data demonstrated that interaction between IPI-O1 and StCWC15 proteins was
275 abolished when the nuclear localization signal of IPI-O1 was mutated, indicating that nuclear
276 localization is important for the interaction. We also performed bimolecular fluorescence
277 complementation (BiFC) to investigate the subcellular localization of interaction between
278 IPI-O1 and StCWC15. The results demonstrated that IPI-O1 interacted with StCWC15
279 proteins in nuclear speckles and the nucleolus (Supplemental Fig. S8). We did not observe
280 fluorescence when testing the interaction between StCWC15 proteins and the IPI-O1^{nls} or
281 Pi04314 (Supplemental Fig. S8). Both the nucleolus and nuclear speckles are cellular
282 structures highly correlated with RNA splicing (Liao and Regev, 2021). While expression of
283 fusion proteins of StCWC15a and StCWC15b with the red fluorescence protein (RFP)
284 demonstrated that StCWC15a primarily localized to the nucleoplasm (91%), the protein was
285 occasionally found in the nucleolus (5%) and nuclear speckles (4%). StCWC15b was
286 distributed similarly and was localized in the nucleoplasm (90%), nucleolus (5%) and nuclear
287 speckles (5%) (Supplemental Fig. S9). To detect StCWC15 subcellular localization changes
288 that may occur in the presence of the IPI-O1 effector, we co-expressed StCWC15a/b-RFP
289 fusion proteins with GFP-IPI-O1 in *N. benthamiana*, with GFP-IPI-O1^{nls} and GFP protein
290 alone as controls. The results showed that StCWC15a protein was re-localized into speckles
291 (63%) or the nucleolus (26%), and that StCWC15b protein was re-localized into speckles
292 (60%) or the nucleolus (25%) when co-expressed with IPI-O1, but not with IPI-O1^{nls} or GFP
293 (Fig. 7E). To further investigate the re-localization of CWC15 during *P. infestans* infection, *N.*
294 *benthamiana* expressing GFP–CWC15a/b was inoculated with zoospores of transgenic *P.*

295 *infestans* isolate 88069 expressing the fluorescent protein RFP. The number of cells with
296 speckle-localized CWC15 near the infected hyphae increased more than in cellsdistant from
297 the infected hyphae (Supplemental Fig. S10). *P. infestans* infection had no effect on nuclear
298 localization of the GFP control (Supplemental Fig. S10). These results suggest that IPI-O1
299 interacts with StCWC15 proteins in the nucleus and induces their re-localization from the
300 nucleoplasm into speckles and the nucleolus.
301
302 **Silencing StCWC15 disrupts *RB*-mediated immunity**
303 To determine the effect of CWC15 on *RB*-mediated immunity, we transiently silenced
304 CWC15, transcription-related factors *PPS7*, (Katou et al., 2005), and splicing-related genrs
305 *SR30*, and *RS2Z32* (Reddy, 2004) in *RB* transgenic *N. benthamiana* followed by transient
306 expression of IPI-O1. Infiltrated areas were assayed for HR elicitation. We found that
307 silencing of *CWC15* resulted in a reduced incidence of HR compared to the EV control, while
308 *PPS7*, *SR30*, or *RS2Z32* silencing had no effect on RB recognition of IPI-O1 (Supplemental
309 Fig. S11A). *SGT1* silencing, known to be required for *RB* function (Bhaskar et al., 2008), also
310 reduced HR incidence compared to the EV control (Supplemental Fig. S11A). The effect of
311 CWC15 on *R* gene function appeared to be specific for *RB*, as silencing of *CWC15* had no
312 effect on the elicitation of HR following co-infiltration of *R1*, *Rpiblb2*, or *R3a* with their
313 corresponding effectors, or following infiltration of elicitor *INF* (Supplemental Fig. S11B).
314 Based on the transient screening results, we further verified the function of *CWC15* by
315 virus-induced gene silencing (VIGS). The TRV-*NbCWC15* silenced plant exhibited small and
316 short morphology compared to wildtype (Supplemental Fig. S12, A and B). Similar to the
317 transiently silenced results, TRV-*NbCWC15* silenced plants were disturbed for the recognition
318 of IPI-O1 by *RB* (Supplemental Fig. S12, C-E). Together, this indicated CWC15 as an
319 interactor of IPI-O1 involved in *RB* activation. To verify the function of potato *CWC15* in
320 *RB*-mediated immunity, we stably silenced *StCWC15* by introducing a hairpin-silencing
321 construct in *RB*-transgenic potato by transformation. We obtained three independent
322 transgenic lines in which *StCWC15* transcription was reduced and a susceptible phenotype
323 was exhibited following inoculation with *P. infestans* when compared to the *RB* transgenic
324 parent potato (Fig. 8, A-D). CWC15 has been reported to regulate alternative splicing in

325 Arabidopsis (Slane et al., 2020). Therefore, we hypothesized that StCWC15 would play a
326 role in *P. infestans*-induced AS of *RB*. To test this, we detected *RB* transcript levels in the
327 highest silencing efficiency line *RB-StCWC15* RNAi#2 following inoculation with *P.*
328 *infestans* isolate JH19. We found that the *RB_CDS/RB_IR* splicing ratio remained constant in
329 the *StCWC15* knockdown plant, while the ratio increased in the *RB* transgenic control plant
330 (Fig. 8E). These data demonstrate that splicing factor CWC15 is involved in regulating *RB*
331 splicing changes during *P. infestans* infection, thus affecting *RB*-mediated immunity in
332 potato.

333 We further silenced *CWC15* using VIGS in *RB*, *RB_CDS* and *Rpi-blb2* transgenic *N.*
334 *benthamiana*. We found that the silencing of *CWC15* significantly impaired IPI-O1 induced
335 HR and resistance to *P. infestans* in the *RB* line. Silencing had no effect on the resistance of
336 *RB_CDS* and *Rpi-blb2* transgenic lines, nor on the HR induced by Avr3a/R3a or INF1 (Fig.
337 8F and Supplemental Fig. S13) This data indicates that CWC15 specifically targets splicing
338 of *RB* and does not affect the function of *RB* once the intron is removed. To validate the role
339 of CWC15 in *RB*-mediated resistance, we complemented *StCWC15* in the TRV-*NbCWC15*
340 silenced *RB* transgenic *N. benthamiana* using silencing-resistant *CWC15* synthetic constructs.
341 These synthetic genes were constructed with shuffled synonymous codons and encode
342 full-length StCWC15a/b (Supplemental Fig. S14A). The results showed that expression of
343 StCWC15a^{syn} and StCWC15b^{syn} rescued the impaired HR and *RB* resistance in TRV
344 silenced-*CWC15* transgenic plants (Fig. 8G and Supplemental Fig. S14B). Immunoblot
345 analysis revealed that expression of StCWC15a^{syn} and StCWC15b^{syn} recovered the
346 expression of CWC15 in silenced *N. benthamiana* (Supplemental Fig. S14, C and D).
347 Collectively, our results indicate that IPI-O1 modulates splicing factor CWC15 to mediate the
348 AS of *RB* and increase the expression level of resistant transcript *RB_CDS*, leading to
349 activation of *RB*-mediated immunity.

350

351 **Regulation of *RB* intron splicing is critical for balancing plant growth and immunity**

352 Our previous results indicated that the intron within *RB* is primarily not spliced in the
353 absence of pathogen infection, leading to a truncated protein that cannot induce immune
354 responses. The presence of pathogen effector IPI-O1 in the nucleus leads to increased intron

splicing and, presumably, increased translation of a full-length RB protein. This regulation suggests that the plant maintains *RB* in a non-spliced state during normal growth perhaps to avoid auto-immunity responses that could impact growth and development. To test this, we generated *RB*, *RB_CDS*, and *RB_IR* transgenic lines in potato cultivar Favorita and assessed their growth characteristics. All three of these genes were driven by a 35S constitutive promoter. In the seedling stage, *RB_CDS* transgenic lines exhibited shorter stem height and root length than non-transformed Favorita, while *RB* and *RB_IR* transgenic lines were not significantly different (Fig. 9, A and B). We also found that *RB_CDS* transgenic potatoes displayed slower growth and dwarf phenotypes compared to the wild-type *RB* transgenic potatoes when grown in pots (Supplemental Fig. S15). We further assessed tuber production and found there was no significant difference of the total number of tubers per plant between any of the transgenic lines and non-transformed Favorita. However, the average yield per plant and the average individual tuber mass was significantly reduced in plants expressing *RB_CDS* compared with Favorita, while these traits in *RB* and *RB_IR* transgenic potatoes were not significantly altered (Fig. 9, C and D). Research has found that accumulation of salicylic acid (SA) in response to biotic stress will affect the growth of plants (Ning et al., 2017; Gao et al., 2021a; Gao et al., 2021b). We compared SA concentrations in *RB* and *RB_CDS* transgenic potatoes with non-transformed wildtype potatoes and found that SA accumulation in the *RB_CDS* transgenic line was higher than in wildtype and *RB* transgenic potatoes (Fig. 9E). The *SARD1* gene is a key regulator for SA synthesis and plant immunity (Zhang et al., 2010). We tested the expression of *SARD1* in transgenic potatoes by RT-qPCR and found it was up-regulated in *RB_CDS* transgenic potatoes compared to wildtype and *RB* transgenic potatoes (Fig. 9F). Transcription of the SA-regulated defense gene *PR1* was also up-regulated in *RB_CDS* transgenic potatoes compared to the wildtype and *RB* transgenic potatoes (Fig. 9G). These results indicate that the sustained expression of *RB_CDS* in the non-infected state leads to continuous activation of SA-mediated defense responses, which likely affects growth and tuber production.

Discussion

Our work has revealed a new model of regulation of plant immunity responses: a

385 pathogen effector (IPI-O1) targets a component of the spliceosome (CWC15) to modulate
386 intron splicing of a plant *NLR* gene (*RB*). This results in increased production of the
387 full-length NLR protein that can further activate immunity in the presence of the same
388 effector. This study implicates the spliceosome as a sensor to surveil pathogen effector
389 activity, and activate plant immunity through proper splicing of an *NLR*. In this model, the
390 plant utilizes alternative intron splicing to regulate expression of the *NLR* to limit
391 inappropriate stress-induced responses during normal growth (Fig. 10). Earlier studies
392 indicate a direct interaction between IPI-O1 and RB (Chen et al., 2012), and that IPI-O1 and
393 RB should be localized to the cytoplasm to induce the HR (Zhao and Song, 2021). Further
394 evidence indicates that IPI-O1 also accumulates in the nucleus (Wang et al., 2018). Together
395 with the data presented here, we propose that IPI-O1 should be present in both the cytoplasm
396 and the nucleus in order to fully activate immunity in the presence of *RB*.

397 Pathogens and plants are eternally entrenched in molecular warfare utilizing an arsenal
398 of microbial effector proteins that manipulate the host to cause disease, and an equally
399 diverse set of host protein receptors that recognize the presence of pathogen effectors to
400 activate immune responses. Given the complexity of possible interactions between host and
401 pathogen molecules, it is no surprise that multiple mechanisms exist to mediate effector
402 recognition and activate resistance. Classical activation models of NLR proteins and effectors
403 include direct recognition, indirect recognition, integrated decoy, and activation traps
404 (Duxbury et al., 2021). The simplest mechanism is direct interaction between NLR proteins
405 and their corresponding effector, leading to changes in protein structure or location that
406 results in resistance activation. An example of this is the flax (*Linum usitatissimum*)
407 resistance proteins L5/L6/L7 that physically interact with effector AvrL567 of flax rust
408 (*Melampsora lini*) to confer resistance (Dodds et al., 2006). The indirect recognition
409 mechanisms are divided into the guardee and the decoy models. In the guardee model, the
410 effectors target a defense-related protein, either through direct binding or protein
411 modification, that is monitored by an NLR protein. When changes in the guarded protein are
412 recognized, this leads to activation of the NLR protein and elicitation of immune responses
413 (Dangl and Jones, 2001). As an example, the Arabidopsis NLR protein RPS2 guards protein
414 RIN4 that is targeted by the pathogen-secreted effector AvrRpt2 (Axtell and Staskawicz,

415 2003). The decoy model is derived from the guardee model, but decoy proteins have no
416 function in host defense or susceptibility in the absence of the NLR protein (van der Hoorn
417 and Kamoun, 2008; Zhou and Chai, 2008). The classical decoy protein in plants is PBL2,
418 which is uridylylated by AvrAC, leading to recognition by the NLR protein ZAR1 (Wang et
419 al., 2015). An integrated decoy is an extension of the decoy model where the effector target is
420 fused directly with the NLR protein, such as the WRKY domain in RRS1 or the HMA
421 domain in RGA5 (Cesari et al., 2014; Maqbool et al., 2015; Sarris et al., 2015). Our results
422 demonstrate an additional mechanism of effector recognition in plants. IPI-O1 is one of
423 multiple *P. infestans* effectors capable of reprogramming genome-wide alternative intron
424 splicing of the host (Huang et al., 2020). The CWC15 protein, a component of the
425 spliceosome, is translocated to the nucleolus in the presence of IPI-O1, leading to splicing of
426 the intron within the *RB* gene. *RB* intron splicing is necessary for the expression of a
427 full-length protein that can activate immunity. The outcome of this model is similar to TAL
428 effector activation traps that result in increased transcription of multiple executor *R* genes
429 (Bogdanove et al., 2010). However, in the case of IPI-O1, *RB* gene expression is likely
430 regulated at the co-transcriptional or post-transcriptional level, and not by transcription
431 activation through promoter binding as it is with TAL effectors.

432 Alternative splicing provides a major source of transcriptome and proteome diversity. In
433 plants, it is estimated that between 42% and 61% of all gene transcripts are alternatively
434 spliced (Filichkin et al., 2010; Lu et al., 2010b; Marquez et al., 2012; Reddy et al., 2013a;
435 Klepikova et al., 2016). AS can increase the protein complexity derived from a single gene
436 and can result in proteins that differ in subcellular localization, stability, or post-translational
437 modifications. AS can also play a role in gene regulation at the RNA level (Jia et al., 2020)
438 and, more specifically, in regulating plant immunity (Reddy, 2007; Huang et al., 2017; Reddy
439 et al., 2020). Several NLR genes undergo AS in the coding sequence or untranslated regions
440 (UTRs; Yang et al., 2014; Lai and Eulgem, 2018). Our data indicate that the *RB* gene
441 produces two different transcripts that encode either a full-length NLR protein that can confer
442 resistance to *P. infestans*, or a truncated protein with only the CC and partial NB domains.
443 Premature termination codon (PTC)-containing transcripts that arise as a result of AS are
444 often subjected to a nonsense-mediated mRNA decay (NMD) process that is intended to

445 prevent their translation (Brogna and Wen, 2009). An analysis of transcripts produced during
446 bacterial infection in Arabidopsis showed that the majority of CC (coiled coil)-NLR (65.1%)
447 and TIR (Toll-like, Interleukin 1)-NLR (81.2%) transcripts exhibit evidence of NMD (Jung et
448 al., 2020). However, transcripts containing PTCs can be used to express the truncated protein
449 or have functional relevance. A truncated NLR protein RBA1 that contains only the TIR
450 domain can still recognize effector HopBA1 and induce cell death (Nishamura et al., 2017).
451 The TIR-NBS truncated protein TN2 associates with and may stabilize calcium-dependent
452 protein kinase5 to regulate defense responses (Liu et al., 2017; Nishimura et al., 2017). Our
453 results indicate that the *RB* gene transcripts that retain the intron are still detectable by
454 RT-PCR and the truncated RB_IR protein is detectable in plants (Fig. 1D), suggesting that the
455 short transcripts are not immediately degraded through NMD. *RB_IR* is predicted to encode a
456 truncated protein of 169 aa and we found that plants transformed with the *RB_IR* construct
457 produced the truncated protein as expected, but did not confer resistance to the pathogen. We
458 hypothesize that this transcript may have other functions for the plant. According to the
459 sequence, this truncated protein still encodes the CC domain of RB. Previous evidence
460 indicates that the CC domain of RB can self-oligomerize (Chen et al., 2012). It remains to be
461 tested whether the truncated CC domain competes with the CC domain from full-length RB
462 to form an inactive oligomerized resistosome during normal growth in order to avoid
463 autoactivation due to RB self-oligomerization.

464 In addition to directly affecting the expression of *NLR* genes, AS plays a more global role
465 in regulating plant disease resistance responses. Arabidopsis *snc1* mutants constitutively
466 activate defense responses and have increased resistance to pathogens (Zhang and Li, 2005).
467 A screen for suppressors of *snc1* revealed two *MOS* (modifier of *snc1*) genes, *MOS4* and
468 *MOS14*, that are involved in mRNA splicing (Palma et al., 2007; Xu et al., 2011). MOS4
469 directly interacts with AtCDC15, a Myb transcription factor, which has significant homology
470 to a component of the spliceosome Nineteen complex, and is essential for NPR4-independent
471 disease resistance signaling (Palma et al., 2007). The MOS14 protein is similar to
472 transportin-SR, which is necessary for nuclear import of serine-arginine (SR) rich proteins
473 (Xu et al., 2011). The SR family of proteins are important in various aspects of RNA splicing
474 (Reddy, 2004; Barta et al., 2008; Long and Caceres, 2008). The *mutation of mos14-1* in

475 Arabidopsis affects splicing of *NLR* gene *SNC1* and *RPS4* and compromises RPS4-dependent
476 immunity and basal resistance to *Pseudomonas syringae* DC3000 (Xu et al., 2011). In
477 Arabidopsis, *P. syringae* introduces small RNAs that silence *SWP73A*, a
478 chromatin-remodeling gene that regulates expression of several *NLRs* through promoter
479 binding and alternative splicing (Huang et al., 2021). *CDC5* has been reported to regulate
480 alternative splicing of *RPS4*, which is important for RPS4 activity (Palma et al., 2007; Zhang
481 and Gassmann, 2007). Although the IPI-O1 effector interacts with CWC15 to regulate the
482 splicing of the *RB* gene, it seems unlikely that *RB* is its specific target. More likely, an
483 IPI-O1/CWC15 complex affects AS at a global level. This is supported by previous data
484 showing that IPI-O1 can regulate AS of immunity-related gene *RLPK* (Huang et al., 2020).
485 The impact of this effector on regulation of plant defense responses will be a focus of future
486 research.

487 For plants, homeostasis between growth and defense is vital for survival and reproduction
488 in nature (He et al., 2022). Research on the role of *NLR* expression in regulating growth
489 versus defense trade-offs in plants has been reported previously (Li et al., 2012; Tsuchiya and
490 Eulgem, 2013; Cui et al., 2020; Huang et al., 2021). NLR proteins are the intracellular
491 immune receptors and activators in plants. The transition between autoinhibited and activated
492 states of NLRs is fine-tuned by intra- and inter-molecular interactions. Over-accumulation of
493 R proteins could lead to autoimmunity (Dinh et al., 2022), whereas insufficient NLR
494 expression could lead to pathogen susceptibility. We found that the intron within the coding
495 sequence of *RB* is alternatively spliced and, under normal growth conditions, transcripts are
496 maintained with the intron retained, leading to a truncated protein. Presumably, this is a
497 strategy to reduce elicitation of immune responses in the absence of an invading pathogen by
498 regulating expression of the full-length RB protein in the plant. This is supported by our
499 results that overexpression of an *RB* gene with the intron removed leads to constitutive
500 expression of defense-related genes, smaller plants, and lowered tuber yield. Following *P.*
501 *infestans* inoculation to introduce the effector IPI-O1, *RB* produces more intron spliced
502 *RB_CDS*, which encodes a full-length NLR protein to provide resistance.

503

Materials and methods

RT-qPCR analysis of *RB* splicing ratio and gene expression

Total RNA was extracted using E.Z.N.A.® Plant RNA Kit (R6827-01, OMEGA) following the manufacturer's instructions and treated with RNase-Free DNase (M6101, Promega) to remove genomic DNA contamination. Approximately 700 ng RNA was used for reverse transcription with HiScript III 1st Strand cDNA Synthesis Kit (R312-01, Vazyme). RT-qPCR was performed with 2μL of 3-fold-diluted cDNA in a total reaction volume of 20μL in technical duplicates using ChamQ Universal SYBR qPCR Master Mix (Q711-02, Vayzme Biotech) with an ABI 7500 Fast Real-time PCR system according to the manufacturer's instructions. PCR conditions were as follows: 95°C for the 30s, followed by 40 cycles of 95°C for 5 s, 60°C for 34 s, and then 95°C for 15 s, 60°C for 1 min, 95°C for 30 s, 60°C for 15s for the melt curve. Relative transcript amount differences were calculated using the $2^{-\Delta\Delta CT}$ method in ABI 7500 System Sequence Detection Software. Three biological replicates were performed and the results showed similar trends.

Gene silencing and complementation in *N. benthamiana*

Virus-induced gene silencing (VIGS) was performed in *N. benthamiana* as previously described (Stam et al., 1997). For VIGS target design, the specific DNA fragments with 300 base pairs (bp) from GFP, *NbCWC15* (Niben101Scf04847g02012.1/Ni-ben101Scf00693g01009.1) predicted by VIGS tool (https://vigs.solgenomics.net/) were cloned into Tobacco Rattle Virus (TRV) construct. The sequences of the targets are listed in Supplemental Data Set S1. The constructs were introduced into *A. tumefaciens* GV3101 by electroporation. Suspensions of *A. tumefaciens* strain GV3101 harboring TRV1 and TRV2 constructs were mixed in a 1:1 ratio in infiltration buffer (10 mM MES, 10 mM $MgCl_2$ pH 5.6, and 150 uM acetosyringone) to a final OD_{600} of 0.4, and then left at room temperature for 2h. TRV2-EV was used as a negative control. Two-week-old *N. benthamiana* plants were infiltrated with *A. tumefaciens* for VIGS assays, and their upper leaves were used 2-3 weeks later. The silencing efficiency was confirmed by RT-qPCR. For the complementation assays, the shuffled synonymous synthetic *StCWC15*

534 sequences were generated by Sangon Biotech and cloned into expression constructs
535 pK7WGF2 with a C-terminal GFP tag. Synthetic proteins were detected by western blot.
536 The 300-bp fragment of *NbPPS7a/b*
537 (*Niben101Scf07798g01001.1*/*Niben101Scf01573g01003.1*), *NbSR30*
538 (*Niben101Scf05298g04002.1*), *NbRS2Z32* (*Niben101Scf07227g00011.1*), *NbSGT1*
539 (*Niben101Scf03241g00015.1*), *NbU1-70ka/b* (*NbS00011208g0006.1*/ *NbS00015731g0004.1*),
540 *NbSF3b1a/b* (Niben101Scf06716g01016.1/ Niben101Scf06128g00004.1), *NbGRP7*
541 (Niben101Scf00215g03004.1) were cloned and ligated into pK7GWIWG2D(II) to generate a
542 hairpin silencing construct. The sequences of the targets are listed in Supplemental Data Set
543 S1. The pK7GWIWG2D(II) empty vector was used as a control. Six- to seven-week *N.*
544 *benthamiana* leaves were infiltrated with GV3101 *A. tumefaciens* strains containing either the
545 silencing construct or empty vector control diluted to an OD_{600}=0.5.
546
547 **Growth of plant material and microbial strains**
548 *Solanum tuberosum* cv. Favorita and transgenic plants were grown on Murashige and
549 Skoog (MS) medium in a growth chamber under 16 h light/8 h dark conditions at a constant
550 temperature of 24 °C and light intensity of 100 μmol m^{-2} s^{-1}. Plants in soil were growth with
551 12 h light/12 h dark conditions at a constant temperature of 22°C and light intensity of 153
552 μmol m^{-2} s^{-1}.
553 *N. benthamiana* plants were grown and maintained in the greenhouse with 16 h light at
554 25°C and 8 h dark at 20°C throughout the experiments. *P. infestans* strains JH19, and 88069^{td},
555 expressing the red fluorescent marker tandem dimer RFP (tdTomato) (Dagdas et al., 2016)
556 were grown on rye sucrose agar (RSA) at 18°C. *P. capsici* strain LT1534 was grown on V8
557 medium at 25°C. *Escherichia coli* strains DH5α, JM109, and BL21 and *A. tumefaciens* strain
558 GV3101 were grown on Luria-Bertani (LB) medium at 37 °C and 30 °C, respectively.
559
560 **Plasmid construction**
561 All primers and plasmids used for cloning and experiments are listed in Supplemental
562 Data Set S2. All the templates used for PCR amplification come from genomic DNA (gDNA)
563 or complementary DNA (cDNA) of *P. infestans* (strain T30-4), *N. benthamiana*, and *Solanum*

tuberosum cv. Favorita using 2 × Phanta Max Master Mix (P515-01, Vazyme Biotech). FastPure Plasmid Mini Kit, FastPure Gel DNA Extraction Mini Kit and ClonExpress Ultra One Step Cloning Kit (Cat No. DC201-01, DC301-01 and C115-01) were used for nucleic acid purification, digestion, and ligation.

Co-immunoprecipitation assays and GST pull-down

The *IPI-O1* gene without the signal peptide was inserted into pK7WGF2 with N-terminal RFP tag using ClonExpress Ultra One Step Cloning Kit (C115-01, Vazyme Biotech), and *StCWC15a/b* were inserted into pK7WGF2 with C-terminal GFP for expression in *N. benthamiana.* Leaves of 6-week-old *N. benthamiana* plants were co-infiltrated with RFP-tagged *IPI-O1*, GFP-tagged *StCWC15a/b*, and the P19 silencing suppressor. Two days after agro-infiltration, the leaves were frozen in liquid nitrogen and ground to powder using a mortar and pestle. Proteins were extracted with extraction buffer (10% [vol/vol] glycerol, 25mM Tris pH=7.5, 1mM EDTA, 150mM NaCl, 2% [wt/vol] PVPP, 10mM DTT, 1×Protease Inhibitor Cocktail (Sigma-Aldrich), 0.1% Tween 20). The samples were centrifuged at 4°C for 20 min at 12,000 × g, and the supernatant was transferred to a new tube. For GFP-IP, 1 mL of supernatant was incubated at 4°C for 2 h with GFP-Trap_A beads (Chromotek, Planegg-Martinsried, Germany). The beads were collected by centrifugation at 800 × g and washed four times in 1 mL washing buffer (25 mM Tris pH=7.5, 150 mM NaCl and 1mM EDTA, 10% [vol/vol] glycerol, 0.1% Tween 20). The beads were boiled for 10 min at 95°C. SDS-PAGE was performed with the supernatant, and co-IP of StCWC15a/b with IPI-O1 was detected using anti-GFP or anti-RFP (Chromotek, Planegg-Martinsried, Germany).

For *in vitro* GST pull-down assays, GST-StCWC15a/b and His-IPI-O1 were expressed in *E. coli* strain BL21. Co-precipitation of StCWC15a/b with IPI-O1 was examined by protein blotting before (input) and after affinity purification (pull-down) using glutathione agarose beads (GE Healthcare). Interactions were detected using anti-GST and anti-His (Abmart).

***P. infestans* and *P. capsici* infection assays**

P. infestans strains were grown on RSA medium plate at 18°C for 14 d. The sporangia were scraped into cold, distilled water and incubated at 4°C for 1-2 h until zoospore release.

594 The zoospore suspension was adjusted to 100 zoospores/μL before inoculation. Ten
595 microliter drops of *P. infestans* zoospores were placed on the abaxial side of detached leaves.
596 The inoculated leaves were kept at 18°C for 4-7 days. The whole potato infection assays used
597 a zoospore suspension sprayed on the plant followed by incubation in a controlled
598 environment chamber at 20°C for 6 days. The infected *N. benthamiana* leaves were stained
599 with trypan blue. Leaves were soaked in trypan blue solution (10 mL 85% lactic acid aqueous,
600 10 mL water-saturated phenol, 10 mL 98% glycerol, 10 mL distilled water, 15 mg trypan blue)
601 overnight. Stained leaves were then transferred into ethanol and incubated at 37°C for 24 h
602 before observation. *P. capsici* strains were grown on V8 medium plate at 25°C for 3 d. Then
603 cut 10 pieces of mycelium with a size of about 2 mm^2 and culture them in V8 liquid medium
604 for 4 days. Discard the culture medium, wash the mycelium with distilled water three times,
605 add distilled water just enough to cover the mycelium, and incubate at 25°C for 12 hours until
606 *P. capsici* produces mature sporangia, placed at 4°C for 20 minutes to stimulate zoospores
607 release.
608
609 **Agroinfiltrations**
610 Construct plasmids were transformed into *A. tumefaciens* strain GV3101 and grown
611 overnight in Luria-Bertani (LB) culture medium with the antibiotics kanamycin and
612 rifampicin at 30°C. Bacteria were harvested by centrifugation at 5000g for 4 min and then
613 resuspended and diluted in an agroinfiltration buffer (10 mM $MgCl_2$, 150 mM acetosyringone,
614 10 mM MES) to an optical density of OD_{600} = 0.01–1.0 depending on the experiments. After
615 2-4 h of incubation at room temperature, they were infiltrated with a needleless syringe into
616 the abaxial side of leaves from 4–5-week-old *N. benthamiana* plants. For the co-expression of
617 multiple constructs, suspensions carrying each construct were thoroughly mixed before
618 infiltration.
619
620 **Confocal microscopy and bimolecular fluorescence complementation (BiFC) assays**
621 Confocal microscopy was performed on N. benthamiana leaf patches post infiltration by
622 LSM 980 laser-scanning microscope with 20×/0.8 or 60×/0.95 objective lens (ZEISS LSM
623 980 with Airyscan2). Parameters that are used for fluorescence detection are GFP/YFP,
624 (excitation 488 nm, emission 505–540 nm), RFP (excitation 514 nm, emission 518–582 nm),
625 DAPI (excitation 405 nm, emission 430–480 nm). Leaves were stained with 2 μg/mL of 4',

626 6-diamidino-2-phenylindole (DAPI) for 5 min to indicate nuclei. ZEISS ZEN Microscope
627 Software was used to process the images.
628 pGTQL1221YC and pGTQL1211YN (nYFP/cYFP) vectors were used for Bimolecular
629 fluorescence complementation (BiFC) assays (Lu et al., 2010a). Coding regions of *IPI-O1*
630 and *IPI-O1*^{nls} without a signal peptide and *StCWC15a/b* were amplified with primers
631 containing attB tails and BP-cloned into pDONR207 (Invitrogen). To generate BiFC
632 constructs, constructs were integrated into destination vectors pGTQL1221YC or
633 pGTQL1211YN by LR recombination using Gateway LR clonase II (Invitrogen). The
634 constructs were transformed into *A. tumefaciens* strain GV3101. Two days after
635 agroinfiltration, the Zeiss 980 laser scanning confocal microscope was used for YFP
636 fluorescence detection.
637
638 **Transformation of potato and RNAi in potato**
639 For generating transgenic potato, the entire *RB* gene sequence (3592 bp), *RB_CDS*
640 transcript (2913 bp), *RB_IR* transcript (507 bp) were cloned into pBinGFP2 binary vector
641 containing the *CaMV35S* promoter. The constructs were transformed into the *A. tumefaciens*
642 strain GV3101. To generate stable transgenic potato plants, stems were used for
643 transformation. Stem segments of *Solanum tuberosum* cv. Favorita were incubated in
644 MS-medium (Murashige and Skoog, 1962). Agrobacterium containing each plasmid was
645 grown and diluted to a cell concentration of OD_{600}=0.5. Stem segments were added and
646 incubated in the dark for 45 mins. After co-incubation, stem segments were transferred to MS
647 solid medium supplemented with 2.5 mg/L zeantinribose, 0.2 mg/L NAA, 0.02 mg/L GA_3 for
648 48 hours. After that, stems were washed with 300mg/L Timentin and transferred to MS solid
649 medium supplemented with 2.5 mg/L zeantinribose, 0.2 mg/L NAA, 0.02 mg/L GA_3 and 200
650 mg/L Timentin for 2 weeks. For callus induction, stems segments were kept on MS solid
651 medium with 2 mg/L zeantinribose, 0.02 mg/L NAA, 0.02 mg/L GA_3, 300 mg/L Timentin
652 and 50 mg/L kanamycin. Every 14 days, stem segments or developing calli were placed onto
653 new medium. After bud initiation formation (following 4-5 transfers), shoots were cut off
654 from the callus and transferred to MS-medium containing 300 mg/L Timentin and 50 mg/L
655 kanamycin.

656 For hairpin RNA interference (RNAi), the chalcone synthase (CHSA) intron was
657 amplified from plasmid pFGC5941 The PCR-amplified 3′StCWC15 cDNA fragments
658 overlapped the 5′ and 3′ end of the CHSA intron from two directions. The overlapped
659 fragment was inserted in the p1300 vector and transformed into *A. tumefaciens* strain
660 GV3101 before potato transformation. Transformation is the same as potato stable
661 overexpression transformation. *StCWC15s* silencing transgenic lines were confirmed by
662 RT-qPCR in buds using the primers indicated in Supplemental Data Set S2.
663
664 **5' RACE**
665 Rapid amplification of cDNA ends (5' RACE) was used to determine the transcripts of
666 the *RB* gene using the SMARTer RACE cDNA Amplification Kit (Clontech) according to the
667 protocol. For synthesis of first-strand cDNA, we designed the *RB* specific primer
668 (Supplemental Data Set S2). Next, we used 10 μM *RB* specific primer and the provided UPM
669 primer in the kit for RACE PCR. Amplification was performed using a touchdown PCR
670 protocol with five cycles of 94°C for 30 s, 72°C for 4 min, then five cycles of 94°C for 30 s,
671 70°C for 30s, 72°C for 4 min, final 25 cycles of 94°C for 30 s, 68°C for 30 s, 72°C for 4 min.
672 The obtained 5′RACE products were gel excised, introduced into the pUC19 vector using
673 in-fusion cloning, and sequenced by Sanger sequencing to detect the transcripts.
674
675
676 **LUC reporter assays**
677 For LUC reporter system assays in *N. benthamiana* leaves, a 1986-bp *RB* fragment
678 including the intron structure was amplified from *RB* transgenic potato (SP951) genomic
679 DNA and fused with *LUC* gene ligated into pCAMBIA1300. Four- or five-week-old *N.*
680 *benthamiana* leaves were infiltrated with Agrobacterium strain GV3101 harboring the
681 indicated constructs resuspended in infiltration buffer for 48 h, after which the leaves were
682 sprayed with 1 mM D-luciferin substrate and incubated for 5 min in the dark. The sprayed
683 leaves were photographed using a Tanon-5200 Multi Chemiluminescent Imaging System
684 (Tanon, China). For quantification of LUC activity, *N. benthamiana* leaf discs were collected
685 at 48 h after infiltration (hpi) and incubated with 1 mM D-luciferin in a 96-well plate, and

686 LUC activity was quantified with the Promega GloMax Navigator microplate luminometer
687 (Promega, USA).
688
689 **Yeast two-hybrid screening**
690 To identify interacting partners with the *P. infestans* effector IPI-O1, a yeast two-hybrid
691 interaction screen was performed by Hybrigenics Services (Évry-Courouronnes, France)
692 using IPI-O1 as a bait in an ULTImate Y2H library constructed from *N. benthamiana*. IPI-O1,
693 encoding amino acids 2-132, was cloned into the inducible pB35 vector as a fusion with
694 GAL4 at the amino terminus. The prey library was prepared in the proprietary pP6
695 Hybrigenics vector. A total of 81.6 million interactions were analyzed and 254 clones were
696 processed by sequencing of the prey inserts. These prey fragments were fused out-of-frame
697 with the Gal4 activation domain (AD) in pP6. However, *Saccharaomyces cerevisiae* are able
698 to translate a percentage of the correct fusion proteins using ribosomal frameshift
699 (Fromont-Racine et al., 1997; Vidal & Legrain, 1999). For this reason, it is possible to
700 identify true interacting proteins from out-of-frame clones.
701
702 **Hypersensitive response phenotype and ion leakage**
703 Hypersensitive cell death during the ETI process was scored at 4 dpi and was quantified
704 using an ion leakage assay (Mittler et al., 1999). Membrane ion leakage was determined by
705 measuring electrolytes leaked from leaf discs. For each measurement, five 9 mm leaf discs
706 were immersed in 5 mL distilled water at room temperature (22-25°C) for 3h. After which,
707 the initial conductivity was measured with Multi-parameter tester (Mettler Toledo S400-K),
708 referred to as value A. Total conductivity was determined after boiling at 95°C for 25 min and
709 cooling to room temperature; this is referred to as value B. The ion leakage was expressed as
710 the percentage of the initial conductivity versus the total conductivity (value A/value B)
711 ×100%.
712
713 **Transcription inhibition assay**
714 Pladienolide B (CAS:445493-23-2) was purchased from Adooq. Pla-B, dissolved in
715 DMSO, was infiltrated into *RB* transgenic *N. benthamiana*. The exact concentration of
716 DMSO was used as control infiltrated in *N. benthamiana*.
717 Lanthanum (III) chloride ($LaCl_3$) (Sigma, CAS: 10099-58-8) was dissolved in water and

718 infiltrated at a concentration of 2 mM.

719

720 **Acknowledgements**

721 We thank Prof. Jiamu Du, Porf. Zhe Wu (Southern University of Science and Technology),
722 Prof. Jiming Jiang (Michigan State University), Prof. Sebastian Schornack (University of
723 Cambridge), Prof. Yan Wang (Nanjing Agriculture University) for helpful discussions.
724 This work was supported by the Chinese National Science Funds Grants (32130088,
725 32102234) and the China Agriculture Research System-potato (CARS-potato, CARS-09-P20).
726 This research was supported in part by the United States Department of Agriculture (USDA)
727 Agricultural Research Service (ARS). Funding was provided through USDA National
728 Institute of Food and Agriculture (NIFA) Plant-Associated Microbes and Plant-Microbe
729 Interactions award number 2014-67013-21593. The findings and conclusions in this
730 publication are those of the author(s) and should not be construed to represent any official
731 USDA or United States Government determination or policy.

732

733 **References**

734

735 Axtell, M.J., and Staskawicz, B.J. (2003). Initiation of RPS2-specified disease resistance in
736 Arabidopsis is coupled to the AvrRpt2-directed elimination of RIN4. Cell 112,
737 369-377.
738 Barta, A., Kalyna, M., and Lorković, Z.J. (2008). Plant SR Proteins and Their Functions. In
739 Nuclear pre-mRNA Processing in Plants, A.S.N. Reddy and M. Golovkin, eds (Berlin,
740 Heidelberg: Springer Berlin Heidelberg), pp. 83-102.
741 Bazin, J., Mariappan, K., Jiang, Y., Blein, T., Voelz, R., Crespi, M., and Hirt, H. (2020). Role
742 of MPK4 in pathogen-associated molecular pattern-triggered alternative splicing in
743 Arabidopsis. PLoS Pathog 16, e1008401.
744 Bhaskar, P.B., Raasch, J.A., Kramer, L.C., Neumann, P., Wielgus, S.M., Austin-Phillips, S.,
745 and Jiang, J. (2008). Sgt1, but not Rar1, is essential for the RB-mediated
746 broad-spectrum resistance to potato late blight. BMC Plant Biol 8, 8.

747 Boevink, P.C., Wang, X., McLellan, H., He, Q., Naqvi, S., Armstrong, M.R., Zhang, W., Hein,
748 I., Gilroy, E.M., and Tian, Z. (2016). A *Phytophthora infestans* RXLR effector targets
749 plant PP1c isoforms that promote late blight disease. Nature Communications 7,
750 10311.
751 Bradeen, J.M., Iorizzo, M., Mollov, D.S., Raasch, J., Kramer, L.C., Millett, B.P.,
752 Austin-Phillips, S., Jiang, J., and Carputo, D. (2009). Higher copy numbers of the
753 potato *RB* transgene correspond to enhanced transcript and late blight resistance levels.
754 Molecular Plant-Microbe Interactions 22, 437-446.
755 Cesari, S., Bernoux, M., Moncuquet, P., Kroj, T., and Dodds, P.N. (2014). A novel conserved
756 mechanism for plant NLR protein pairs: the "integrated decoy" hypothesis. Front
757 Plant Sci 5, 606.
758 Champouret, N., Bouwmeester, K., Rietman, H., Lee, T.v.d., Maliepaard, C., Heupink, A.,
759 Vondervoort, P.J.I.v.d., Jacobsen, E., Visser, R.G.F., Vossen, E.A.G.v.d., Govers, F.,
760 and Vleeshouwers, V.G.A.A. (2009). *Phytophthora infestans* Isolates Lacking Class I
761 *ipiO* Variants Are Virulent on *Rpi-blb1* Potato. MPMI 22, 1535-1545.
762 Chen, M., and Manley, J.L. (2009). Mechanisms of alternative splicing regulation: insights
763 from molecular and genomics approaches. Nat Rev Mol Cell Biol 10, 741-754.
764 Chen, Y., Liu, Z., and Halterman, D.A. (2012). Molecular determinants of resistance
765 activation and suppression by Phytophthora infestans effector IPI-O. PLoS Pathogen
766 8, e1002595.
767 Cheng, Y.T., Li, Y., Huang, S., Huang, Y., Dong, X., Zhang, Y., and Li, X. (2011). Stability of
768 plant immune-receptor resistance proteins is controlled by SKP1-CULLIN1-F-box
769 (SCF)-mediated protein degradation. Proc Natl Acad Sci U S A 108, 14694-14699.
770 Couto, D., and Zipfel, C. (2016). Regulation of pattern recognition receptor signalling in
771 plants. Nat Rev Immunol 16, 537-552.
772 Cretu, C., Agrawal, A.A., Cook, A., Will, C.L., Fekkes, P., Smith, P.G., Luhrmann, R., Larsen,
773 N., Buonamici, S., and Pena, V. (2018). Structural Basis of Splicing Modulation by
774 Antitumor Macrolide Compounds. Mol Cell 70, 265-273 e268.
775 Cui, C., Wang, J.-J., Zhao, J.-H., Fang, Y.-Y., He, X.-F., Guo, H.-S., and Duan, C.-G. (2020).
776 A Brassica miRNA Regulates Plant Growth and Immunity through Distinct Modes of

Action. Mol. Plant 13, 231-245.

Cui, H., Tsuda, K., and Parker, J.E. (2015). Effector-Triggered Immunity: From Pathogen Perception to Robust Defense. Annual Review of Plant Biology 66, 487-511.

Dagdas, Y.F., Belhaj, K., Maqbool, A., Chaparro-Garcia, A., Pandey, P., Petre, B., Tabassum, N., Cruz-Mireles, N., Hughes, R.K., Sklenar, J., Win, J., Menke, F., Findlay, K., Banfield, M.J., Kamoun, S., and Bozkurt, T.O. (2016). An effector of the Irish potato famine pathogen antagonizes a host autophagy cargo receptor. Elife 5.

Dangl, J.L., and Jones, J.D.G. (2001). Plant pathogens and integrated defence responses to infection. Nature 411, 826-833.

Deng, Y., Zhai, K., Xie, Z., Yang, D., Zhu, X., Liu, J., Wang, X., Qin, P., Yang, Y., Zhang, G., Li, Q., Zhang, J., Wu, S., Milazzo, J., Mao, B., Wang, E., Xie, H., Tharreau, D., and He, Z. (2019). Epigenetic regulation of antagonistic receptors confers rice blast resistance with yield balance. Science 355, 962-965.

Dinesh-Kumar, S.P., and Baker, B.J. (2000). Alternatively spliced N resistance gene transcripts: Their possible role in tobacco mosaic virus resistance. Proc. Natl Acad. Sci. USA 97, 1908–1913.

Dinh, H.X., Singh, D., Gomez de la Cruz, D., Hensel, G., Kumlehn, J., Mascher, M., Stein, N., Perovic, D., Ayliffe, M., Moscou, M.J., Park, R.F., and Pourkheirandish, M. (2022). The barley leaf rust resistance gene *Rph3* encodes a predicted membrane protein and is induced upon infection by avirulent pathotypes of *Puccinia hordei*. Nature Communications 13, 2386.

Dodds, P.N., and Rathjen, J.P. (2010). Plant immunity: towards an integrated view of plant-pathogen interactions. Nature reviews. Genetics 11, 539-548.

Dodds, P.N., Lawrence, G.J., Catanzariti, A.-M., Teh, T., Wang, C.-I.A., Ayliffe, M.A., Kobe, B., and Ellis, J.G. (2006). Direct protein interaction underlies gene-for-gene specificity and coevolution of the flax resistance genes and flax rust avirulence genes. Proceedings of the National Academy of Sciences 103, 8888-8893.

Duxbury, Z., Wu, C.H., and Ding, P. (2021). A Comparative Overview of the Intracellular Guardians of Plants and Animals: NLRs in Innate Immunity and Beyond. Annu Rev Plant Biol 72, 155-184.

807 Filichkin, S.A., Priest, H.D., Givan, S.A., Shen, R., Bryant, D.W., Fox, S.E., Wong, W.-K.,
808 and Mockler, T.C. (2010). Genome-wide mapping of alternative splicing in
809 Arabidopsis thaliana. Genome Research 20, 45-58.
810 Gao, M., He, Y., Yin, X., Zhong, X., Yan, B., Wu, Y., Chen, J., Li, X., Zhai, K., Huang, Y.,
811 Gong, X., Chang, H., Xie, S., Liu, J., Yue, J., Xu, J., Zhang, G., Deng, Y., Wang, E.,
812 Tharreau, D., Wang, G.L., Yang, W., and He, Z. (2021a). Ca(2+) sensor-mediated
813 ROS scavenging suppresses rice immunity and is exploited by a fungal effector. Cell
814 184, 5391-5404 e5317.
815 Gao, W., Liu, Y., Huang, J., Chen, Y., Chen, C., Lu, L., Zhao, H., Men, S., and Zhang, X.
816 (2021b). MES7 Modulates Seed Germination via Regulating Salicylic Acid Content
817 in Arabidopsis. Plants (Basel) 10.
818 Halterman, D., Wei, F., and Wise, R. (2003). Powdery mildew induced *Mla* mRNAs are
819 alternatively spliced and contain multiple upstream open reading frames. Plant
820 Physiol 131, 558-567.
821 Halterman, D.A., and Wise, R.P. (2006). Upstream open reading frames of the barley Mla13
822 powdery mildew resistance gene function co-operatively to down-regulate translation.
823 Molecular Plant Pathology 7, 167-176.
824 Haverkort, A.J., Struik, P.C., Visser, R.G.F., and Jacobsen, E. (2009). Applied Biotechnology
825 to Combat Late Blight in Potato Caused by Phytophthora Infestans. Potato Research
826 52, 249-264.
827 He, Z., Webster, S., and He, S.Y. (2022). Growth-defense trade-offs in plants. Current
828 Biology 32, R634-R639.
829 Huang, C.Y., Rangel, D.S., Qin, X., Bui, C., Li, R., Jia, Z., Cui, X., and Jin, H. (2021). The
830 chromatin-remodeling protein BAF60/SWP73A regulates the plant immune receptor
831 NLRs. Cell Host Microbe 29, 425-434 e424.
832 Huang, J., Lu, X., Wu, H., Xie, Y., Peng, Q., Gu, L., Wu, J., Wang, Y., Reddy, A.S.N., and
833 Dong, S. (2020). *Phytophthora* effectors modulate genome-wide alternative splicing
834 of host mRNAs to reprogram plant immunity. Molecular plant 13, 1470-1484.
835 Huang, J., Gu, L., Zhang, Y., Yan, T., Kong, G., Kong, L., Guo, B., Qiu, M., Wang, Y., Jing,
836 M., Xing, W., Ye, W., Wu, Z., Zhang, Z., Zheng, X., Gijzen, M., Wang, Y., and Dong,

837 S. (2017). An oomycete plant pathogen reprograms host pre-mRNA splicing to
838 subvert immunity. Nature Communications 8.
839 Jia, J., Long, Y., Zhang, H., Li, Z., Liu, Z., Zhao, Y., Lu, D., Jin, X., Deng, X., Xia, R., Cao,
840 X., and Zhai, J. (2020). Post-transcriptional splicing of nascent RNA contributes to
841 widespread intron retention in plants. Nature Plants 6, 780-788.
842 Jones, J.D., and Dangl, J.L. (2006). The plant immune system. Nature 444, 323-329.
843 Jung, H.W., Panigrahi, G.K., Jung, G.Y., Lee, Y.J., Shin, K.H., Sahoo, A., Choi, E.S., Lee, E.,
844 Man Kim, K., Yang, S.H., Jeon, J.S., Lee, S.C., and Kim, S.H. (2020).
845 Pathogen-associated molecular pattern-triggered immunity involves proteolytic
846 degradation of core nonsense-mediated mRNA decay factors during the early defense
847 response. Plant Cell 32, 1081-1101.
848 Kamoun, S., and Smart, C.D. (2005). Late Blight of Potato and Tomato in the Genomics Era.
849 Plant Disease 89, 692-699.
850 Kamoun, S., Furzer, O., Jones, J.D.G., Judelson, H.S., Ali, G.S., Dalio, R.J.D., Roy, S.G.,
851 Schena, L., Zambounis, A., Panabieres, F., Cahill, D., Ruocco, M., Figueiredo, A.,
852 Chen, X.R., Hulvey, J., Stam, R., Lamour, K., Gijzen, M., Tyler, B.M., Grunwald, N.J.,
853 Mukhtar, M.S., Tome, D.F.A., Tor, M., Van den Ackerveken, G., McDowell, J., Daayf,
854 F., Fry, W.E., Lindqvist-Kreuze, H., Meijer, H.J.G., Petre, B., Ristaino, J., Yoshida, K.,
855 Birch, P.R.J., and Govers, F. (2015). The Top 10 oomycete pathogens in molecular
856 plant pathology. Molecular Plant Pathology 16, 413-434.
857 Karki, H.S., Jansky, S.H., and Halterman, D.A. (2021). Screening of Wild Potatoes Identifies
858 New Sources of Late Blight Resistance. Plant Disease 105, 368-376.
859 Katou, S., Yoshioka, H., Kawakita, K., Rowland, O., Jones, J.D.G., Mori, H., and Doke, N.
860 (2005). Involvement of PPS3 Phosphorylated by Elicitor-Responsive
861 Mitogen-Activated Protein Kinases in the Regulation of Plant Cell Death. Plant
862 Physiology 139, 1914-1926.
863 Klepikova, A.V., Kasianov, A.S., Gerasimov, E.S., Logacheva, M.D., and Penin, A.A. (2016).
864 A high resolution map of the Arabidopsis thaliana developmental transcriptome based
865 on RNA-seq profiling. The Plant Journal 88, 1058-1070.
866 Kotake, Y., Sagane, K., Owa, T., Mimori-Kiyosue, Y., Shimizu, H., Uesugi, M., Ishihama, Y.,

867 Iwata, M., and Mizui, Y. (2007). Splicing factor SF3b as a target of the antitumor
868 natural product pladienolide. Nat Chem Biol 3, 570-575.
869 Lai, Y., and Eulgem, T. (2018). Transcript-level expression control of plant NLR genes. Mol
870 Plant Pathol 19, 1267-1281.
871 Li, F., Pignatta, D., Bendix, C., Brunkard, J.O., Cohn, M.M., Tung, J., Sun, H., Kumar, P., and
872 Baker, B. (2012). MicroRNA regulation of plant innate immune receptors.
873 Proceedings of the National Academy of Sciences USA 109, 1790-1795.
874 Li, X., Kapos, P., and Zhang, Y. (2015). NLRs in plants. Curr Opin Immunol 32, 114-121.
875 Liao, S.E., and Regev, O. (2021). Splicing at the phase-separated nuclear speckle interface: a
876 model. Nucleic Acids Res 49, 636-645.
877 Liu, N., Hake, K., Wang, W., Zhao, T., Romeis, T., and Tang, D. (2017).
878 CALCIUM-DEPENDENT PROTEIN KINASE5 Associates with the Truncated NLR
879 Protein TIR-NBS2 to Contribute to exo70B1-Mediated Immunity. Plant Cell 29,
880 746-759.
881 Long, Jennifer C., and Caceres, Javier F. (2008). The SR protein family of splicing factors:
882 master regulators of gene expression. Biochemical Journal 417, 15-27.
883 Lu, Q., Tang, X., Tian, G., Wang, F., Liu, K., Nguyen, V., Kohalmi, S.E., Keller, W.A., Tsang,
884 E.W.T., Harada, J.J., Rothstein, S.J., and Cui, Y. (2010a). Arabidopsis homolog of the
885 yeast TREX-2 mRNA export complex: components and anchoring nucleoporin. The
886 Plant Journal 61, 259-270.
887 Lu, T., Lu, G., Fan, D., Zhu, C., Li, W., Zhao, Q., Feng, Q., Zhao, Y., Guo, Y., Li, W., Huang,
888 X., and Han, B. (2010b). Function annotation of the rice transcriptome at
889 single-nucleotide resolution by RNA-seq. Genome Research 20, 1238-1249.
890 Maqbool, A., Saitoh, H., Franceschetti, M., Stevenson, C.E., Uemura, A., Kanzaki, H.,
891 Kamoun, S., Terauchi, R., and Banfield, M.J. (2015). Structural basis of pathogen
892 recognition by an integrated HMA domain in a plant NLR immune receptor. Elife 4.
893 Marquez, Y., Brown, J.W.S., Simpson, C., Barta, A., and Kalyna, M. (2012). Transcriptome
894 survey reveals increased complexity of the alternative splicing landscape in
895 Arabidopsis. Genome Research 22, 1184-1195.
896 Ning, Y., Liu, W., and Wang, G.L. (2017). Balancing Immunity and Yield in Crop Plants.

897 Trends Plant Sci 22, 1069-1079.
898 Nishimura, M.T., Anderson, R.G., Cherkis, K.A., Law, T.F., Liu, Q.L., Machius, M.,
899 Nimchuk, Z.L., Yang, L., Chung, E.H., El Kasmi, F., Hyunh, M., Osborne Nishimura,
900 E., Sondek, J.E., and Dangl, J.L. (2017). TIR-only protein RBA1 recognizes a
901 pathogen effector to regulate cell death in Arabidopsis. Proceedings of the National
902 Academy of Sciences USA 114, E2053-E2062.
903 Ofir, G., Herbst, E., Baroz, M., Cohen, D., Millman, A., Doron, S., Tal, N., Malheiro, D.B.A.,
904 Malitsky, S., Amitai, G., and Sorek, R. (2021). Antiviral activity of bacterial TIR
905 domains via immune signalling molecules. Nature 600, 116-120.
906 Palma, K., Zhao, Q., Cheng, Y.T., Bi, D., Monaghan, J., Cheng, W., Zhang, Y., and Li, X.
907 (2007). Regulation of plant innate immunity by three proteins in a complex conserved
908 across the plant and animal kingdoms. Genes & Development 21, 1484-1493.
909 Paluchowska, P., Sliwka, J., and Yin, Z. (2022). Late blight resistance genes in potato
910 breeding. Planta 255, 127.
911 Reddy, A.S. (2007). Alternative splicing of pre-messenger RNAs in plants in the genomic era.
912 Annu Rev Plant Biol 58, 267-294.
913 Reddy, A.S.N. (2004). Plant serine/arginine-rich proteins and their role in pre-mRNA splicing.
914 Trends in Plant Science 9, 541-547.
915 Reddy, A.S.N., Marquez, Y., Kalyna, M., and Barta, A. (2013a). Complexity of the
916 Alternative Splicing Landscape in Plants. The Plant Cell 25, 3657-3683.
917 Reddy, A.S.N., Marquez, Y., Kalyna, M., and Barta, A. (2013b). Complexity of the
918 Alternative Splicing Landscape in Plants The Plant Cell 25, 3657-3683.
919 Reddy, A.S.N., Huang, J., Syed, N.H., Ben-Hur, A., Dong, S., and Gu, L. (2020). Decoding
920 co-/post-transcriptional complexities of plant transcriptomes and epitranscriptome
921 using next-generation sequencing technologies. Biochemical Society Transactions 48,
922 2399-2414.
923 Sanchez-Martin, J., Widrig, V., Herren, G., Wicker, T., Zbinden, H., Gronnier, J., Sporri, L.,
924 Praz, C.R., Heuberger, M., Kolodziej, M.C., Isaksson, J., Steuernagel, B., Karafiatova,
925 M., Dolezel, J., Zipfel, C., and Keller, B. (2021). Wheat Pm4 resistance to powdery
926 mildew is controlled by alternative splice variants encoding chimeric proteins. Nat

927 Plants 7, 327-341.
928 Sarris, P.F., Duxbury, Z., Huh, S.U., Ma, Y., Segonzac, C., Sklenar, J., Derbyshire, P., Cevik,
929 V., Rallapalli, G., Saucet, S.B., Wirthmueller, L., Menke, F.L.H., Sohn, K.H., and
930 Jones, J.D.G. (2015). A Plant Immune Receptor Detects Pathogen Effectors that
931 Target WRKY Transcription Factors. Cell 161, 1089-1100.
932 Sheth, N., Roca, X., Hastings, M.L., Roeder, T., Krainer, A.R., and Sachidanandam, R. (2006).
933 Comprehensive splice-site analysis using comparative genomics. Nucleic Acids Res
934 34, 3955-3967.
935 Slane, D., Lee, C.H., Kolb, M., Dent, C., Miao, Y., Franz-Wachtel, M., Lau, S., Macek, B.,
936 Balasubramanian, S., Bayer, M., and Jurgens, G. (2020). The integral spliceosomal
937 component CWC15 is required for development in Arabidopsis. Sci Rep 10, 13336.
938 Song, J., Bradeen, J.M., Naess, S.K., Raasch, J.A., Wielgus, S.M., Haberlach, G.T., Liu, J.,
939 Kuang, H., Austin-Phillips, S., Buell, C.R., Helgeson, J.P., and Jiang, J. (2003). Gene
940 RB cloned from Solanum bulbocastanum confers broad spectrum resistance to potato
941 late blight. Proc Natl Acad Sci U S A 100, 9128-9133.
942 Stam, M., Mol, J.N.M., and Kooter, J.M. (1997). The silence of genes in transgenic plants.
943 Annals of Botany 79, 3-12.
944 Sukarta, O.C.A., Zheng, Q., Slootweg, E.J., Mekken, M., Mendel, M., Putker, V., Bertran, A.,
945 Brand, A., Overmars, H., Pomp, R., Roosien, J., Boeren, S., Smant, G., and Goverse,
946 A. (2022). GLYCINE-RICH RNA-BINDING PROTEIN 7 potentiates
947 effector-triggered immunity through an RNA recognition motif. Plant Physiol 189,
948 972-987.
949 Sun, H., Jiao, W.B., Krause, K., Campoy, J.A., Goel, M., Folz-Donahue, K., Kukat, C.,
950 Huettel, B., and Schneeberger, K. (2022). Chromosome-scale and haplotype-resolved
951 genome assembly of a tetraploid potato cultivar. Nat Genet 54, 342-348.
952 Tsuchiya, T., and Eulgem, T. (2013). An alternative polyadenylation mechanism coopted to
953 the Arabidopsis RPP7 gene through intronic retrotransposon domestication.
954 Proceedings of the National Academy of Sciences USA 110, E3535-3543.
955 Van de Weyer, A.L., Monteiro, F., Furzer, O.J., Nishimura, M.T., Cevik, V., Witek, K., Jones,
956 J.D.G., Dangl, J.L., Weigel, D., and Bemm, F. (2019). A Species-Wide Inventory of

957 NLR Genes and Alleles in Arabidopsis thaliana. Cell 178, 1260-1272 e1214.
958 van der Hoorn, R.A., and Kamoun, S. (2008). From Guard to Decoy: a new model for
959 perception of plant pathogen effectors. Plant Cell 20, 2009-2017.
960 van der Vossen, E., Sikkema, A., Hekkert, B., Gros, J., Stevens, P., Muskens, M., Wouters, D.,
961 Pereira, A., Stiekema, W., and Allefs, S. (2003). An ancient R gene from the wild
962 potato species Solanum bulbocastanum confers broad-spectrum resistance to
963 Phytophthora infestans in cultivated potato and tomato. Plant J 36, 867-882.
964 Vleeshouwers, V.G., Rietman, H., Krenek, P., Champouret, N., Young, C., Oh, S.K., Wang,
965 M., Bouwmeester, K., Vosman, B., Visser, R.G., Jacobsen, E., Govers, F., Kamoun, S.,
966 and Van der Vossen, E.A. (2008). Effector genomics accelerates discovery and
967 functional profiling of potato disease resistance and phytophthora infestans avirulence
968 genes. PLoS One 3, e2875.
969 Wan, R., Bai, R., Zhan, X., and Shi, Y. (2020). How Is Precursor Messenger RNA Spliced by
970 the Spliceosome? Annu Rev Biochem 89, 333-358.
971 Wang, G., Roux, B., Feng, F., Guy, E., Li, L., Li, N., Zhang, X., Lautier, M., Jardinaud, M.F.,
972 Chabannes, M., Arlat, M., Chen, S., He, C., Noel, L.D., and Zhou, J.M. (2015). The
973 Decoy Substrate of a Pathogen Effector and a Pseudokinase Specify
974 Pathogen-Induced Modified-Self Recognition and Immunity in Plants. Cell Host
975 Microbe 18, 285-295.
976 Wang, J., Hu, M., Wang, J., Qi, J., Han, Z., Wang, G., Qi, Y., Wang, H.W., Zhou, J.M., and
977 Chai, J. (2019). Reconstitution and structure of a plant NLR resistosome conferring
978 immunity. Science 364.
979 Wang, L., Yang, T., Wang, B., Lin, Q., and Yu, F. (2020). RALF1-FERONIA complex affects
980 splicing dynamics to modulate stress responses and growth in plants. Science
981 Advances 6, eaaz1622.
982 Wang, S., McLellan, H., Bukharova, T., He, Q., Murphy, F., Shi, J., Sun, S., van Weymers, P.,
983 Ren, Y., Thilliez, G., Wang, H., Chen, X., Engelhardt, S., Vleeshouwers, V., Gilroy,
984 E.M., Whisson, S.C., Hein, I., Wang, X., Tian, Z., Birch, P.R.J., and Boevink, P.C.
985 (2018). Phytophthora infestans RXLR effectors act in concert at diverse subcellular
986 locations to enhance host colonization. Journal of Experimental Botany 70, 343-356.

987 Wu, Z., Zhu, D., Lin, X., Miao, J., Gu, L., Deng, X., Yang, Q., Sun, K., Zhu, D., Cao, X.,
988 Tsuge, T., Dean, C., Aoyama, T., Gu, H., and Qu, L.J. (2016). RNA Binding Proteins
989 RZ-1B and RZ-1C Play Critical Roles in Regulating Pre-mRNA Splicing and Gene
990 Expression during Development in Arabidopsis. Plant Cell 28, 55-73.
991 Xu, F., Xu, S., Wiermer, M., Zhang, Y., and Li, X. (2012). The cyclin L homolog MOS12 and
992 the MOS4-associated complex are required for the proper splicing of plant resistance
993 genes. The plant jouranl 70, 916-928.
994 Xu, S., Zhang, Z., Jing, B., Gannon, P., Ding, J., Xu, F., Li, X., and Zhang, Y. (2011).
995 Transportin-SR is required for proper splicing of resistance genes and plant immunity.
996 PLOS Genetics 7, e1002159.
997 Yang, S., Tang, F., and Zhu, H. (2014). Alternative splicing in plant immunity. International
998 journal of molecular sciences 15, 10424-10445.
999 Zhang, F., Fang, H., Wang, M., He, F., Tao, H., Wang, R., Long, J., Wang, J., Wang, G.L., and
1000 Ning, Y. (2022). APIP5 functions as a transcription factor and an RNA-binding
1001 protein to modulate cell death and immunity in rice. Nucleic Acids Res 50,
1002 5064-5079.
1003 Zhang, X.-C., and Gassmann, W. (2007). Alternative splicing and mRNA levels of the disease
1004 resistance gene *RPS4* are induced during defense responses. Plant Physiology 145,
1005 1577-1587.
1006 Zhang, Y., and Li, X. (2005). A putative nucleoporin 96 is required for both basal defense and
1007 constitutive resistance responses mediated by *suppressor of npr1-1, constitutive 1*.
1008 The Plant Cell 17, 1306-1316.
1009 Zhang, Y., Xu, S., Ding, P., Wang, D., Cheng, Y.T., He, J., Gao, M., Xu, F., Li, Y., Zhu, Z., Li,
1010 X., and Zhang, Y. (2010). Control of salicylic acid synthesis and systemic acquired
1011 resistance by two members of a plant-specific family of transcription factors. Proc
1012 Natl Acad Sci U S A 107, 18220-18225.
1013 Zhao, J., and Song, J. (2021). NLR immune receptor RB is differentially targeted by two
1014 homologous but functionally distinct effector proteins. Plant Communications 2.
1015 Zhou, J.-M., and Chai, J. (2008). Plant pathogenic bacterial type III effectors subdue host
1016 responses. Current Opinion in Microbiology 11, 179-185.

1017

1018 **Figure Legends**

1019 **Figure 1. The *RB* intron is alternatively spliced.**

1020 **(A)** Gene model and splicing isoforms of *RB*. 5' and 3' UTRs are shaded grey. The intron is
1021 denoted by a black line. The asterisk shows the location of a premature termination codon.
1022 The arrows indicate the primers used in (B). Red letters in *RB_IVS* denote mutations to
1023 change the intron splicing recognition sites. **(B)** RT-PCR of *RB* and *RB_IVS* splicing mutant
1024 from transgenic *S. tuberosum* cv. Favorita and transgenic *N. benthamiana*. *RB_IR* is 995bp,
1025 and *RB_CDS* is 316bp. cDNA of Favorita and wildtype *N. benthamiana* were used as
1026 negative controls. *StEF1α* and *NbEF1α* were used as internal controls. **(C)** Diagrams showing
1027 the domains present in each of the predicted proteins produced from transcripts. **(D)**
1028 Expression of Myc-tagged fusions of RB, RB_CDS, and RB_IR in *N. benthamiana* was
1029 confirmed by western blotting using an anti-Myc antibody. The asterisk stands for the
1030 predicted protein RB RB_CDS and RB_IR. Equal protein loading was visualized by Ponceau
1031 S staining.

1032

1033 **Figure 2. *RB* intron splicing is specifically induced following *P. infestans* inoculation.**

1034 **(A)** RT-PCR of *RB_IR* or *RB_CDS* variants in *RB* transgenic potato following inoculation
1035 with water (mock), *P. infestans* JH19 or *P. capsici* LT1534. *StEF1α* was used as the internal
1036 control. **(B)** Splicing ratio of *RB* in transgenic potato following inoculation with water (mock),
1037 *P. infestans* JH19, or *P. capsici* LT1534. Transcript levels were detected by RT-qPCR and
1038 normalized to *RB_CDS* following mock treatment at 0 dpi. Bars represent the mean ± SD
1039 from three independent replicates. ns, no significant difference. One asterisk denotes a
1040 significant difference at $P<0.05$, and three asterisks denotes a significant difference at
1041 $P<0.001$ using a two-way ANOVA with Tukey's test.

1042

1043 **Figure 3. Intron retention in *RB* results in susceptibility to *P. infestans*.**

1044 **(A)** Zoospore suspension of *P. infestans* strain JH19 was used to inoculate *RB*, *RB_CDS*,
1045 *RB_IR* and *RB_IVS* transgenic potato plants at a concentration of 15,000 zoospores/mL.
1046 Plants were photographed at 5 dpi. The numbers represent the ratio of resistant plants
1047 compared to all inoculated plants. Bar = 5 cm. **(B)** Zoospore suspension of *P. infestans* strain

1048 JH19 was drop-inoculated on detached leaves of *RB* transgenic potato expressing the
1049 indicated gene variants. The infected leaves were photographed at 4 dpi. The numbers
1050 represent the ratio of resistant leaves compared to all inoculated leaves. Bars represent the
1051 percent infected area of the detached leaves. The data represents the mean ± SD from 12
1052 replications. Different letters above bars denote a significant difference at P<0.001 using a
1053 two-way ANOVA with Dunn's test.
1054
1055 **Figure 4. Spliceosome activity is necessary for *RB*-mediated resistance to *P. infestans*.**
1056 **(A)** Trypan blue staining of *RB* transgenic *N. benthamiana* following agroinfiltration of
1057 RNAi-hairpin constructs and inoculation with *P. infestans* zoospores. EV = empty vector
1058 control. Leaves were photographed at 5 dpi. **(B)** Lesion areas (cm^2) of inoculated leaves in
1059 (A). Data represents the mean ± SD from 8 replicates. Different letters above bars denotes a
1060 significant difference at P<0.001 using a one-way ANOVA with Dunn's test. **(C)** Splicing
1061 ratio of *RB* in *RB* transgenic *N. benthamiana* following agroinfiltration of RNAi-hairpin
1062 constructs for 1 day and inoculation with *P. infestans* zoospores. RNA was extracted 2 days
1063 after pathogen inoculation. Transcript levels were detected by RT-qPCR and normalized to
1064 *RB_CDS* in RNAi-EV and following mock treatment. Bars represent the mean ± SD in three
1065 independent replicates. **(D)** Agroinfiltration of IPI-O1 in *RB* and *RB_CDS* transgenic *N.*
1066 *benthamiana* with DMSO (control), 1 μM splicing modulator Pladienolide B (Pla-B), or 30
1067 μM Pla-B. Cell death was visually assessed and photographed at 4 dpi (left). Numbers show
1068 the ratio of infiltrated areas with cell death compared to the all infiltrated areas. Electrolyte
1069 leakage was monitored by conductivity measurements following the same treatments (right).
1070 Data represents the mean ± SD from 8 replications. **(E)** Splicing ratio of *RB* in *RB* transgenic
1071 *N. benthamiana* following treatment with DMSO (control), 1 μM Pla-B, or 30 μM Pla-B and
1072 inoculation with *P. infestans* zoospores at 2 dpi by RT-qPCR. ns, no significant difference.
1073 Three asterisks denotes a statistical difference at P<0.001 using a two-way ANOVA with
1074 Tukey's test.
1075
1076 **Figure 5. IPI-O1 induces *RB* intron splicing.**
1077 **(A)** Schematic diagram of the *RB_LUC* alternative splicing reporter system. The genomic

1078 sequence of *RB* was fused with the luciferase (*LUC*) gene to construct 35S::*RB-LUC*. Intron
1079 retention introduces a premature termination codon (PTC) and no production of the luciferase
1080 reporter. Intron splicing leads to a full-length RB-LUC protein with luciferase activity. The
1081 *35S*::*RB_CDS-LUC* construct with the intron removed produces a full-length RB-LUC
1082 protein with luciferase activity regardless of intron splicing activity. The *35S*::*LUC* construct
1083 is a positive control. **(B)** Results of co-expression of the reporters with multiple splicing
1084 regulatory effectors (SRE) that we previously identified (Huang et al., 2020). LUC activity
1085 was quantified at 48 hpi. Relative LUC activity was normalized to the activity of the
1086 *35S*::*RB_CDS-LUC* construct with mock treatment. Data represents the mean ± SD from 24
1087 replications. Different letters above each bar represent a significant difference at $P<0.001$
1088 using a two-way ANOVA with Dunn's test. **(C)** GFP-tagged SRE fusion protein expression in
1089 *N. benthamiana* was confirmed by western blotting using an anti-GFP antibody. Protein
1090 loading was visualized by Ponceau S staining.
1091
1092 **Figure 6. Nuclear localization of IPI-O1 is necessary for *RB* intron splicing.**
1093 **(A)** Schematic diagrams at the top show the location of alanine replacements within the
1094 nuclear localization signal of IPI-O1. GFP-IPI-O1 and GFP-IPI-O1^{nls} were expressed in *N.*
1095 *benthamiana* leaves for 48 h before imaging, Scale bar = 20 μm. **(B)** Subcellular localization
1096 of IPI-O1 and IPI-O1^{nls}. Bars represent the number of times that GFP was detected in the
1097 nucleoplasm or nucleolus following infiltration of GFP-IPI-O1 and GFP-IPI-O1^{nls}. Data
1098 represents the mean ± SD of three replicates. **(C)** Expression of GFP-tagged fusions of
1099 IPI-O1 and IPI-O1^{nls} in *N. benthamiana* was confirmed by protein blotting using an anti-GFP
1100 antibody. Protein loading was visualized by Ponceau S staining. **(D)** On the left are visual
1101 examples and incidence ratios of hypersensitive cell death responses following
1102 agroinfiltration of IPI-O1 and IPI-O1^{nls} in leaves of *RB*, *RB_CDS*, and *RB_IR* transgenic *N.*
1103 *benthamiana*. Cell death was visually assessed and photographed at 4 dpi. The right panel
1104 shows results of electrolyte leakage assays of infiltrated areas. Data represents the mean ± SD
1105 of 12 replications. **(E)** Splicing ratio of *RB* in *RB* transgenic *N. benthamiana* following
1106 agroinfiltration of IPI-O1 and IPI-O1^{nls} at 2 dpi by RT-qPCR. Bars represent the mean ± SD
1107 of three independent replicates. **(F)** Results of co-expression of RB_LUC reporters with

1108 mock, GFP, IPI-O1 and IPI-O1^{nls} in *N. benthamiana* leaves by agroinfiltration. LUC activity
1109 was quantified at 2 dpi. Relative LUC activity was normalized to the activity of the 35S::*LUC*
1110 construct with mock treatment. Data represents the mean ± SD of 30 replications. For all
1111 graphs, ns = no significant difference and three asterisks denotes a statistical difference at
1112 P<0.001 using a two-way ANOVA with Tukey's test.
1113
1114 **Figure 7. IPI-O1 physically interacts with splicing factor CWC15.**
1115 **(A)** Yeast-two hybrid interaction between IPI-O1 and CWC15 homologs from *N.*
1116 *benthamiana*. Yeast transformants were spotted as 10-fold serial dilutions on SD medium
1117 without leucine and tryptophan (SD–2), or without histidine, leucine, adenine, and tryptophan
1118 (SD–4). Yeast cells were photographed 2-3 days after plating. Empty BD and AD plasmids
1119 (EV) were used as controls. Experiments were performed at least three times with similar
1120 results. **(B)** Immunoprecipitation (IP) of StCWC15a/b-GFP with RFP-IPI-O1, RFP-IPI-O1^{nls},
1121 or RFP-Pi04314 following agroinfiltration in *N. benthamiana* leaves. Expression of
1122 constructs in the leaves is indicated by +. Markers are indicated on the right, and the Ponceau
1123 S stain was used to show levels of protein loading. **(C)** *In vitro* pull-down assay using the
1124 GST-tagged StCWC15a/b to immunoprecipitate IPI-O1 or IPI-O1^{nls}. Input and
1125 GST-pull-down proteins were visualized by protein blotting using anti-GST and anti-His
1126 antibodies. Asterisks (*) indicate the protein bands that correspond to the expected size of
1127 CWC15a/b. **(D)** IPI-O1, but not IPI-O1^{nls}, can interact with CWC15 homologs in potato.
1128 Yeast transformants were spotted as 10-fold serial dilutions on SD medium without leucine
1129 and tryptophan (SD–2), or without histidine, leucine, adenine, and tryptophan (SD–4). Yeast
1130 cells were photographed 2-3 days later. BD and AD are bait and prey EVs, respectively.
1131 Experiments were performed at least three times with similar results. **(E)** IPI-O1 co-localizes
1132 with StCWC15a/b in nuclear speckles and the nucleolus. GFP-IPI-O1, GFP-IPI-O1^{nls}, and
1133 GFP alone were transiently co-expressed with StCWC15a/b-RFP by agroinfiltration in *N.*
1134 *benthamiana*. The left image is from the GFP channel, the middle image is from the RFP
1135 channel, and the right image is the overlay of the GFP and RFP channels. Numbers represent
1136 the frequency of cells showing indicated StCWC15 subcellular localization compared to the
1137 total StCWC15-positive cells in 25mm^2 discs from three biological replicates. Graphs show

1138 the fluorescence intensity profiles across the arrows in the merged images. Bar = 5μm.

1139

1140 **Figure 8. Silencing *StCWC15* disrupts *RB*-mediated resistance.**

1141 **(A)** Whole plants were spray-inoculated (left) and detached leaves were drop-inoculated
1142 (right) with zoospores of *P. infestans* strain JH19 in *RB* and *RB-StCWC15* RNAi transgenic
1143 potato. Bar = 3 cm. The number represents the frequency of leaves showing resistance
1144 compared to all inoculated leaves. **(B)** Zoospore suspension of *P. infestans* strain JH19 was
1145 drop-inoculated on detached leaves of *RB* and *RB-StCWC15* RNAi transgenic potato. The
1146 infected leaves were photographed at 4 dpi. The numbers represent the ratio of resistant
1147 leaves compared to all inoculated leaves. **(C)** Relative expression of *StCWC15a/b* in three
1148 RNAi transformed lines compared to *RB* transgenic potato. Bars represent the mean ± SD of
1149 three independent replicates. Three asterisks designate a statistical difference from the *RB*
1150 control at P<0.001 using a two-way ANOVA with Tukey's test. **(D)** Infection ratio of *P.*
1151 *infestans* JH19 on *RB* and *RB-StCWC15* RNAi transgenic potato lines. Data represents the
1152 mean ± SD from 10 replications. Different letters denote a significance difference at P<0.001
1153 using a one-way ANOVA with Dunn's test. **(E)** Splicing ratio of *RB* in *RB-StCWC15* RNAi
1154 transgenic potato line #2 following inoculation with *P. infestans* zoospores at 2 dpi by
1155 RT-qPCR. Bars represent the mean ± SD from three independent replicates. ns=no significant
1156 difference and three asterisks denotes a statistical difference at P<0.001 using a two-way
1157 ANOVA with Tukey's test. **(F)** *NbCWC15* was silenced by VIGS in *RB*, *RB_CDS*, and
1158 *Rpi_blb2* transgenic *N. benthamiana* and inoculated with *P. infestans* JH19 on detached
1159 leaves. Photos (top) and lesion areas (bottom) were recorded at 5 dpi. Lesion area data
1160 represents the mean ± SD from 18 replications. **(G)** Complementation of *RB* function caused
1161 by *CWC15* silencing in *N. benthamiana* via synthetic *StCWC15* constructs (*StCWC15a/b*^{syn}).
1162 Agrobacterium expressing *StCWC15a/b*^{syn} constructs were infiltrated into *NbCWC15* silenced
1163 *RB* transgenic *N. benthmiana*, then inoculated with *P. infestans* JH19 zoospores. Photos and
1164 lesion areas were recorded at 5 dpi. Data represent the mean ± SD from 8 replications.
1165 Different letters denote a significance difference at P<0.001 using one-way ANOVA with
1166 Dunn's test.

1167

1168 **Figure 9. Alternative intron splicing of *RB* balances plant growth and immunity.**
1169 **(A)** Photos of 21-day-old wild-type (WT) Favorita and *RB*, *RB_CDS*, and *RB_IR* transgenic
1170 tissue culture plants. Bar = 1 cm. **(B)** Average stem height and root length measurements of
1171 Favorita (WT) and 21-day-old transgenic potato tissue culture plants. Bars represent the mean
1172 ± SD from 15 tissue culture plants. **(C)** Tubers of Favorita (WT) and transgenic plants.
1173 Tubers were harvested and photographed 8 to 10 weeks after tissue culture plants were
1174 transplanted. Bar = 1 cm. **(D)** Average tuber yield, average individual tuber mass, and average
1175 number of tubers from greenhouse grown plants. Measurements were taken at 8 to 10 weeks
1176 after tissue culture plants were transplanted. Bars represent the mean ± SD from 15
1177 replications of 3 independent lines for each genotype. **(E)** Total salicylic acid (SA) content in
1178 Favorita (WT) and transgenic *RB* and *RB_CDS* lines without pathogen inoculation. FW, fresh
1179 weight. Bars represent the mean ± SD from three independent replicates. **(F-G)** Relative
1180 expression of *SARD1* (F) and *PR1* (G) in the indicated transgenic potato as determined by
1181 RT-qPCR. Bars represent the mean ± SD from three independent replicates. For all graphs,
1182 different letters represent a statistical difference at P<0.001 using one-way ANOVA with
1183 Dunn's test.
1184
1185 **Fig.10 Schematic model of the *P. infestans*-host pathosystem related to resistance gene**
1186 ***RB* and effector IPI-O1**.
1187 During normal growth (left), CWC15 proteins (grey triangles) are maintained in the
1188 nucleoplasm and *RB* transcripts exist primarily with the intron retained (*RB_IR*). This results
1189 in the production of a truncated, non-functional RB protein that supports growth over
1190 immunity. Following *P. infestans* infection, effector IPI-O1 is introduced into the plant cell
1191 and translocated to the nucleus, leading to a re-localization of CWC15 from the nucleoplasm
1192 to the nucleolus and speckles. This results in increased splicing of the *RB* intron (*RB_CDS*),
1193 resulting in production of a full-length RB protein that can elicit immunity.
1194
1195 **Supplemental Figure S1**. ***RB* undergoes AS and produces two transcript isoforms.**
1196 Schematic of two transcripts of *RB* amplified using 5′-rapid amplification of cDNA ends
1197 (5′-RACE). UPM primer is Universal Primer A Mix, GSP primer is gene specific primer of

RB. The white vertical lines represent single nucleotide polymorphisms that appeared in the sequencing results.

Supplemental Figure S2. ***RB* intron splicing is induced following *P. infestans* inoculation.**
(A) The relative transcription level of *RB* is modified following *P. infestans* but not *P. capsici* inoculation. Quantitative PCR with reverse transcription (RT–qPCR) analysis was performed using isoform-specific primers (Supplemental Data Set S2) to measure the transcript levels of two isoforms. **(B)** Total *RB* transcription levels do not change significantly during infection. RT–qPCR analysis was performed using primers (Supplemental Data Set S2) located in Exon1. For all graphs, bars represent the mean ± SD from three independent replicates. ns = no significant difference and three asterisks denotes a statistical difference at P<0.001 using a two-way ANOVA with Tukey's test.

Supplemental Figure S3. Intron retention in *RB* results in susceptibility to *P. infestans*.
(A) Zoospores of *P.infestans* strain JH19 were inoculated on detached transgenic *N. benthamiana* leaves expressing the indicated gene variants. On the top, leaves were stained with trypan blue and photographed at 5 dpi. Below, lesion areas were calculated using Image J. Data represents the mean ± SD from 21 inoculations from three independent experimental replicates. Different shapes indicate biological replicates. **(B)** Indicated transgenic *N. benthamiana* leaves were agroinfiltrated with IPI-O1 or GFP. On the top, cell death was visually assessed and photographed at 4dpi. The numbers represent incidence ratios of hypersensitive cell death responses. Below shows results of electrolyte leakage assays of infiltrated areas. Data represents the mean ± SD from 9 replications. For all graphs, different letters above each bar represent a statistical difference at P<0.001 using a two-way ANOVA with Dunn's test.

Supplemental Figure S4. Spliceosome activity is necessary for *RB*-mediated resistance to *P. infestans*.
(A) Agroinfiltrations of the indicated RNAi-hairpin constructs to silence *U1-70K*, *SF3B1* and

1228 *GRP7* in *N. benthamiana*, followed by co-agroinfiltration of the indicated *Avr/R* gene
1229 combinations. Cell death was visually assessed and photographed at 4 dpi. The numbers
1230 represent incidence ratios of hypersensitive cell death responses. **(B)** Electrolyte leakage
1231 assay of cell death in (A). Data represents the mean ± SD from 8 replications. Different
1232 letters above each bar represent a significant difference at P<0.001 using a two-way ANOVA
1233 with Dunn's test. **(C)** Results of RT–qPCR to demonstrate the silencing efficiency of RNAi
1234 constructs targeting silencing factors (SFs). Transcript levels of each gene were calculated
1235 relative to the RNAi-EV control. Bars represent the mean ± SD from three independent
1236 replicates. Three asterisks denotes a statistical difference at P<0.001 using a two-way
1237 ANOVA with Tukey's test. **(D)** Transcript levels of *RB_CDS* and *RB_IR* mRNAs following
1238 agroinfiltration of RNAi-hairpin constructs for 1 day and inoculation with *P. infestans*
1239 zoospores. RNA was extracted 2 days after pathogen inoculation. RT-qPCR analysis was
1240 performed using isoform-specific primers to measure the transcript levels of the two isoforms.
1241 Bars represent the mean ± SD from three independent replicates. **(E)** Transcript levels of
1242 *RB_CDS* and *RB_IR* mRNAs in *RB* transgenic *N. benthamiana* following treatment with
1243 DMSO (control), 1 μM Pla-B, or 30 μM Pla-B and inoculation with *P. infestans* zoospores at
1244 2 dpi by RT-qPCR. Bars represent the mean ± SD from three independent replicates.
1245
1246 **Supplemental Figure S5. Luciferase assay to monitor *RB* intron splicing following**
1247 ***P.infestans* inoculation.**
1248 **(A)** Representative photo of a *N. benthamiana* leaf infiltrated with agrobacterium carrying
1249 (clockwise) *RB-LUC*, *LUC*, empty vector (EV) control, or *RB_CDS-LUC*. One day after
1250 agroinfiltration, the infiltrated regions were treated with *P. infestans* or water (mock). The
1251 LUC activity was detected at 1 dpi. **(B)** The graph on the right shows results of 30 individual
1252 leaf discs isolated from leaves agroinfiltrated with each indicated construct followed by
1253 treatment with *P. infestans* or water. LUC activity measurement data represents the mean ±
1254 SD from 30 individual leaf discs from 3 experimental replicates. Relative *LUC* activity was
1255 normalized to the activity of the *35S::LUC* construct with mock treatment. ns = no significant
1256 difference and three asterisks denotes a statistical difference at P<0.001 using a two-way
1257 ANOVA with Tukey's test.

1258

1259 **Supplemental Figure S6. *RB* intron splicing and *RB*-mediated hypersensitive response is**
1260 **specific to expression of IPI-O1 but not other SREs.**
1261 On the left, transcript levels of *RB_IR* and *RB_CDS* were determined by RT-PCR following
1262 agroinfiltration of SRE proteins into leaves of *RB* transgenic *N. benthamiana*. In the middle,
1263 data represent relative intensity of RT-PCR products normalized with internal control
1264 *NbEF1α*. Intensities of the bands were quantified by Image J software, and the relative
1265 abundances of *RB* isoforms are relative to *RB_CDS* at 0 dpi. Bars represent the mean ± SD
1266 from three independent replicates. ns = no significant difference and three asterisks denotes a
1267 statistical difference at P<0.001 using a two-way ANOVA with Tukey's test. On the right are
1268 representative photos of the cell death phenotypes of SRE expression in *RB* transgenic (Nb^{RB})
1269 and wildtype *N. benthamiana* (*Nb*). The numbers represent incidence ratios of cell death
1270 responses.
1271

1272 **Supplemental Figure S7. The splicing factor CWC15 is conserved in potato populations.**
1273 **(A)** Alignment comparing CWC15a and CWC15b in double-monoploid potato DM-1-3. **(B)**
1274 Alignment comparing several CWC15 homologs in different potato cultivars and wild
1275 species. Individual amino acids are depicted in color scheme, degree of overall amino acid
1276 conservation is shown both as line plot and sequence logo. Peptide sequences of CWC15
1277 orthologues were extracted from published potato pan-genome (Tang et al., 2022). All
1278 selected protein sequences were aligned by R-msa packages (Version 1.33.0) in ClustalW
1279 method, and visualized by Jalview (Verion 2.11.0). All the CWC15 sequences used in the
1280 analysis were listed in the Data Set S3.
1281

1282 **Supplemental Figure S8. IPI-O1 interacts with StCWC15a/b, but IPI-O1^{nls} cannot.**
1283 IPI-O1 interacts with StCWC15 in the nucleolus and nuclear speckles. Split-YFP/BiFC of
1284 IPI-O1 or IPI-O1^{nls} and Pi04314 with StCWC15a and b using fluorescence imaging. Samples
1285 were stained with 2 ug/mL DAPI to indicate the nucleus. Numbers represent the frequency of
1286 cells showing YFP fluorescence compared to the total number of cells in the 25mm^2 discs
1287 from three biological replicates. Bar = 5 μm.

1288

1289 **Supplemental Figure S9. StCWC15 is localized in the nucleoplasm.**

1290 **(A)** StCWC15a/b-RFP were expressed in *N. benthamiana* leaves for 48 h before imaging.
1291 Numbers represent the frequency of subcellular localization in indicated cellular structure
1292 compared to the total fluorescent cells in the 25mm^2 range. Bar = 5 μm. **(B)** Immunoblot
1293 analysis of protein in co-localization experiment. RFP tag fusions with StCWC15a/b were
1294 confirmed by protein blotting using an anti-RFP antibody. Protein loading is visualized by
1295 Ponceau S staining. GFP tagged fusions with IPI-O1, IPI-O1^{nls} and GFP proteins were
1296 confirmed by protein blotting using an anti-GFP antibody.

1297

1298 **Supplemental Figure S10**. **Nuclear speckle accumulation of StCWC15 is mediated by *P.***
1299 ***infestans* during infection.**

1300 **(A)** Images are representative of the different patterns observed in GFP–StCWC15
1301 re-localization from the nucleoplasm to speckles. Nucleolar GFP–StCWC15 fluorescence
1302 near the haustoriated cells detected in speckles (upper panel) while in cells distant from the
1303 haustoriated cells, it remained in the nucleoplasm (lower panel). Images are representative of
1304 the GFP protein localization pattern during *P. infestans* infection. Bar =5 μm. **(B)** Data
1305 represents the number of CWC15-positive speckles during *P. infestans* infection. Bars
1306 represent the mean ± SD of 10 replications from three independent replicates. ns = no
1307 significant difference and three asterisks denotes a statistical difference at P<0.001 using a
1308 one-way ANOVA with Tukey's test.

1309

1310 **Supplemental Figure S11**. **Splicing factor CWC15 is specifically involved in**
1311 ***RB*-mediated hypersensitive response.**

1312 **(A)** Silencing of *CWC15* leads to loss of *RB*-mediated HR. IPI-O1 was co-expressed with the
1313 indicated RNAi constructs in *RB* transgenic *N. benthamiana*. Numbers represent the
1314 incidence ratios of hypersensitive cell death responses. Infiltrated areas were photographed 4
1315 dpi. Electrolyte leakage was monitored by conductivity measurements following the same
1316 treatments (bottom). Data represents the mean ± SD from 12 replications. Different letters
1317 designate a significant difference from the empty vector (EV) control at P<0.001. **(B)** The

designated Avr/R gene combinations were co-agroinfiltrated in *N. benthamiana* leaves following silencing of *CWC15*. The HR phenotype was photographed at 4 dpi. The numbers represent incidence ratios of cell death responses (upper). Below shows the results of electrolyte leakage assays of infiltrated areas. Data represents the mean ± SD from 12 replications. ns = no significant difference and three asterisks denotes a statistical difference at P<0.001 using two-way ANOVA with Tukey's test.

Supplemental Figure S12. *CWC15* silencing in *N. benthamiana* by VIGS showed deficiency in growth and immunity.

(A) Schematic diagram showing the fragments used in VIGS constructs. **(B)** The morphology of *NbCWC15* silencing in *N. benthamiana*. Two-week-old *N. benthamiana* plants were infiltrated with agrobacterium carrying TRV: EV, TRV: 5'*NbCWC15*, TRV: 3'*NbCWC15* and TRV: *PDS*, respectively. The photo was taken 3 weeks after infiltration. Bar = 3 cm. **(C, D)** HR induced by IPI-O1 and RB was impaired in *NbCWC15* silenced *N. benthamiana*. (C) 3' *NbCWC15* or 5' *NbCWC15* silencing has disturbed the recognition of IPI-O1 by RB. Hypersensitive cell death phenotypes were photographed at 4 dpi. The numbers represent incidence ratios of hypersensitive cell death responses. **(D)** Electrolyte leakage from the infiltrated leaf discs was measured as a percentage of leakage from boiled discs at 4 dpi. Data represents the mean ± SD from 10 replications. Three asterisks denote a statistical difference at P<0.001 using a one-way ANOVA with Tukey's test. **(E)** Silencing efficiency of *NbCWC15* in *N. benthamiana*. Bars represent mean ± SD of three independent replicates. Two asterisks denote a statistical difference at P<0.05 using two-way ANOVA with Tukey's test.

Supplemental Figure S13. *CWC15* silencing has no effect on *RB_CDS* recognition of IPI-O1.

(A) *CWC15* silencing impairs RB/IPI-O1 induced HR and not RB_CDS/IPI-O1, R3a/Avr3a, or INF1. R gene/effector combinations and INF1 were agroinfiltrated into *NbCWC15*-silenced *N. benthmiana* leaves. Photos of HR phenotypes were taken at 4 dpi. The numbers represent incidence ratios of hypersenisitve cell death responses. **(B)** Quantification

1348 of cell death by measuring electrolyte leakage at 4 dpi. Bars represent the mean ± SD from 12
1349 replications. ns=no significant difference and three asterisks denotes a statistical difference at
1350 P<0.001 using a two-way ANOVA with Tukey's test.
1351
1352
1353 **Supplemental Figure S14 StCWC15 synthetic sequences complement *CWC15* silencing**
1354 **causing *RB*-mediated immunity deficient.**
1355 **(A)** Schematic representation of VIGS and complementation design. The region from
1356 460~696bp of *NbCWC15* was cloned into VIGS construct TRV2-3'*NbCWC15* for silencing.
1357 Synonymous substitutions were introduced into the synthetic StCWC15 ($StCWC15^{syn}$)
1358 without changing the protein sequence. The nucleotide and protein sequence alignments
1359 indicate the synonymous changes in the synthetic variant. **(B)** Expression of
1360 silencing-resistant synthetic StCWC15 ($StCWC15a^{syn}$/ $StCWC15b^{syn}$) rescues *RB*–mediated
1361 HR in *NbCWC15*-silenced *N. benthamiana* plants. GFP and StCWC15a and StCWC15b were
1362 used as controls. Below shows results of electrolyte leakage assays of infiltrated areas at 4 dpi.
1363 The number represents incidence ratios of cell death responses. Bars represent the mean ± SD
1364 from 12 replications. Three asterisks denotes a statistical difference from the control at
1365 P<0.001 using a two-way ANOVA with Tukey's test. **(C-D)** Immunoblot analysis of
1366 StCWC15a/b, $StCWC15a^{syn}$/$StCWC15b^{syn}$ in EV (C) and *CWC15*-silenced (D) plants.
1367 C-terminal GFP-tagged StCWC15 variants were transiently expressed in VIGS control and
1368 *CWC15*-silenced *N. benthamiana.* Protein loading is visualized by Ponceau S staining.
1369
1370 **Supplemental Figure S15**. *RB_CDS* transgenic plant exhibit slowed growth.
1371 **(A)** Photos of cv. Favorita expressing wildtype *RB* ($Favorita^{RB}$) or *RB_CDS* ($Favorita^{RB_CDS}$)
1372 from initial transplanting (0d) to 75 days after transplanting. Bar = 3cm. **(B)** The height of the
1373 transgenic plants graphed over time. Data points combine measurements from 5 individual
1374 transgenic plants. Data represent the mean ± SD from 3 replicates. Statistical differences
1375 among the samples were analyzed with a one-way ANOVA with Dunn's test (P<0.001).

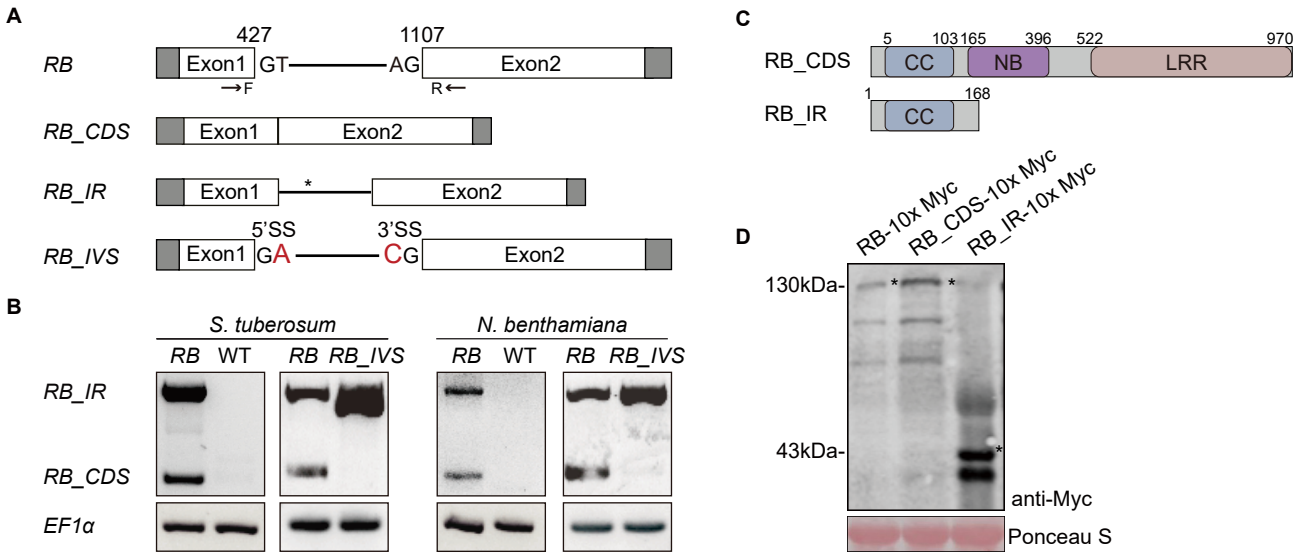

Figure 1. The *RB* intron is alternatively spliced.

(A) Gene model and splicing isoforms of *RB*. 5' and 3' UTRs are shaded grey. The intron is denoted by a black line. The asterisk shows the location of a premature termination codon. The arrows indicate the primers used in (B). Red letters in *RB_IVS* denote mutations to change the intron splicing recognition sites. **(B)** RT-PCR of *RB* and *RB_IVS* splicing mutant from transgenic *S. tuberosum* cv. Favorita and transgenic *N. benthamiana*. *RB_IR* is 995bp, and *RB_CDS* is 316bp. cDNA of Favorita and wildtype *N. benthamiana* were used as negative controls. *StEF1α* and *NbEF1α* were used as internal controls. **(C)** Diagrams showing the domains present in each of the predicted proteins produced from transcripts. **(D)** Expression of Myc-tagged fusions of *RB*, *RB_CDS*, and *RB_IR* in *N. benthamiana* was confirmed by western blotting using an anti-Myc antibody. The asterisk stands for the predicted protein RB RB_CDS and RB_IR. Equal protein loading was visualized by Ponceau S staining.

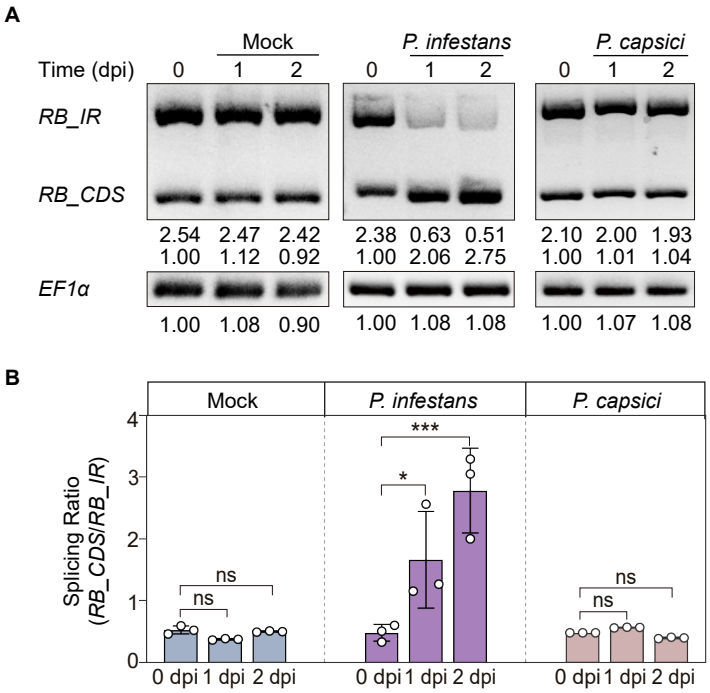

Figure 2. *RB* intron splicing is specifically induced following *P. infestans* inoculation.
(A) RT-PCR of variants *RB_IR* or *RB_CDS* in *RB* transgenic potato following inoculation with water (mock), *P. infestans* JH19 or *P. capsici* LT1534. *StEF1α* was used as the internal control. **(B)** Splicing ratio of *RB* in transgenic potato following inoculation with water (mock), *P. infestans* JH19, or *P. capsici* LT1534. Transcript levels were detected by RT-qPCR and normalized to *RB_CDS* following mock treatment at 0 dpi. Bars represent the mean ± SD from three independent replicates. ns = no significant difference, one asterisk denotes a significant difference at P<0.05, and three asterisks denotes a significant difference at P<0.001 using a two-way ANOVA with Tukey's test.

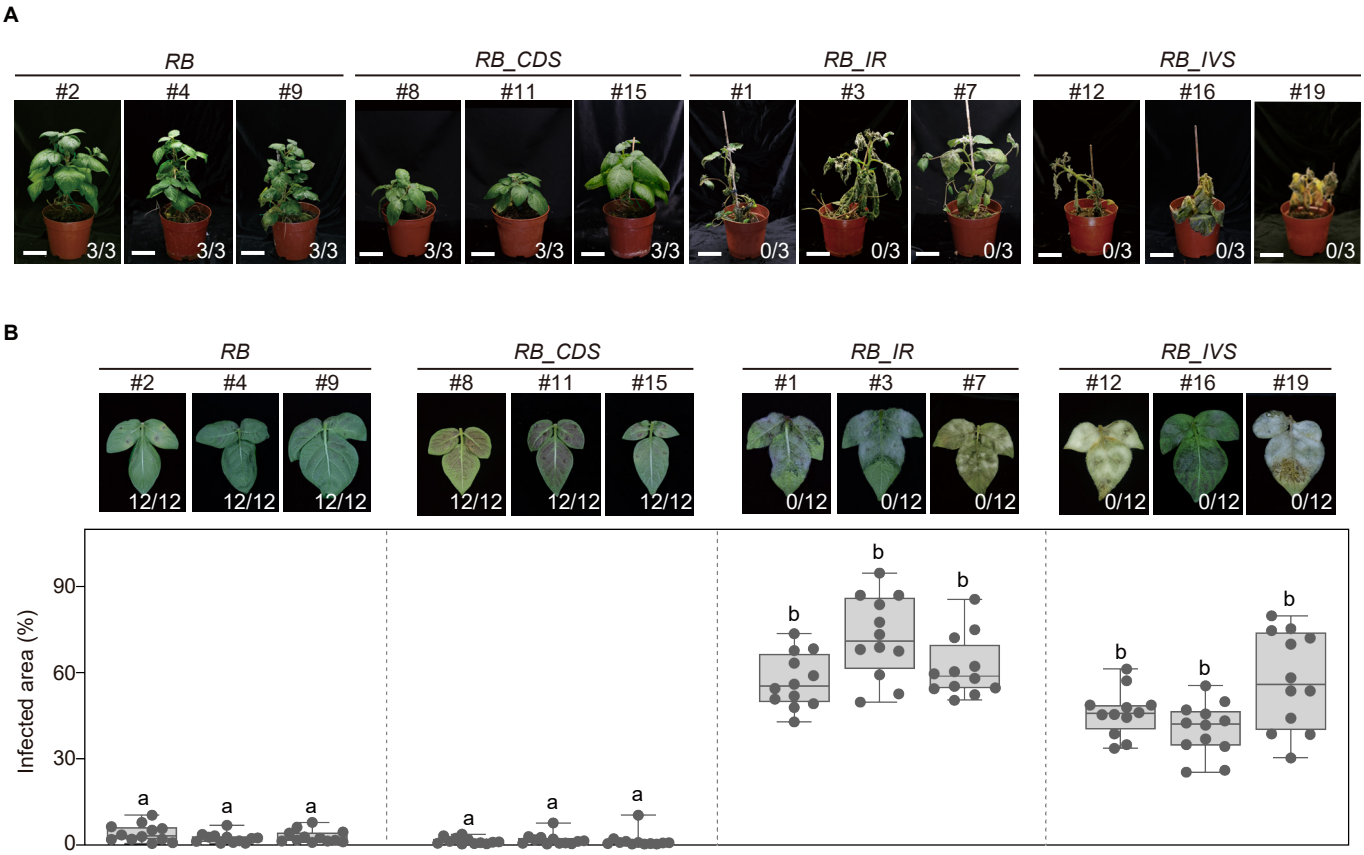

Figure 3. Intron retention in *RB* results in susceptibility to *P. infestans.*
(A) Zoospore suspension of *P. infestans* strain JH19 was used to inoculate *RB*, *RB_CDS*, *RB_IR* and RB^{IVS} transgenic potato plants at a concentration of 15,000 zoospores/ml . Plants were photographed at 5 dpi. The numbers represent the ratio of resistant plants compared to all inoculated plants. Bar = 5 cm. **(B)** Zoospore suspension of *P. infestans* strain JH19 was drop-inoculated on detached leaves of *RB* transgenic potato expressing the indicated gene variants. The infected leaves were photographed at 4 dpi. The numbers represent the ratio of resistant leaves compared to all inoculated leaves. Bars represent the percent infected area of the detached leaves. The data represents the mean ± SD from 12 replications. Different letters above bars denote a significant difference at P<0.001 using a two-way ANOVA with Dunn's test..

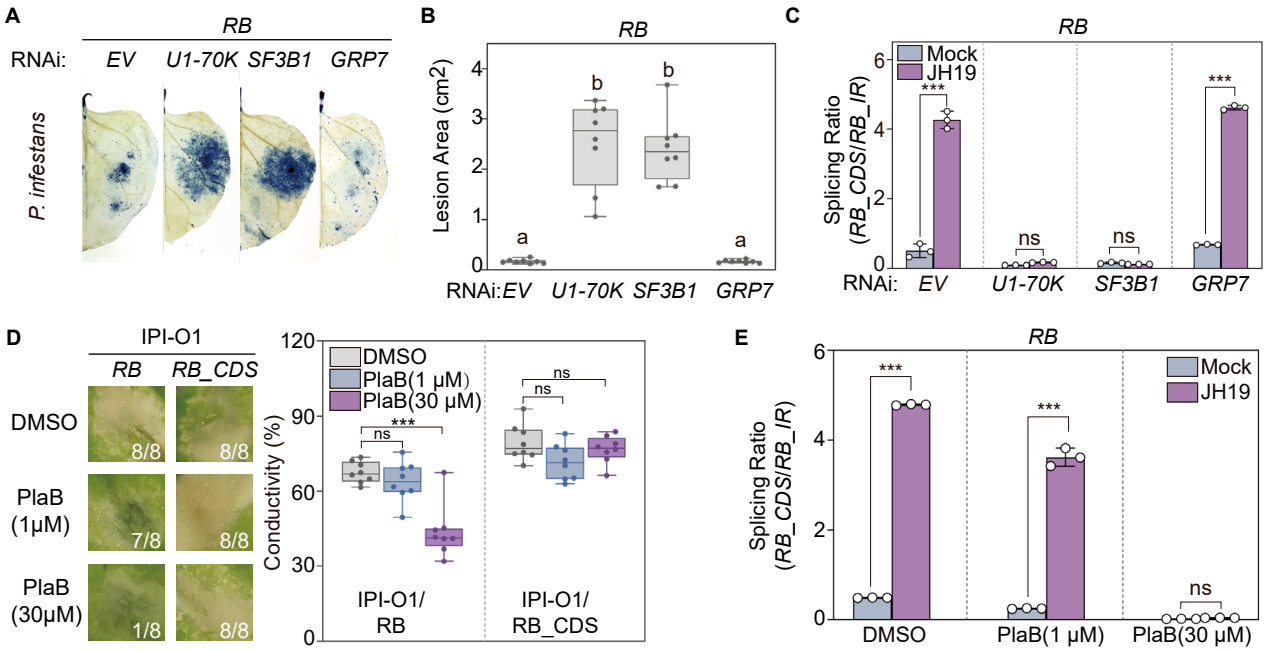

Figure 4. Spliceosome activity is necessary for *RB*-mediated resistance to *P. infestans*.
(A) Trypan blue staining of *RB* transgenic *N. benthamiana* following agroinfiltration of RNAi-hairpin constructs and inoculation with *P. infestans* zoospores. EV = empty vector control. Leaves were photographed at 5 dpi. **(B)** Lesion areas (cm^2) of inoculated leaves in (A). Data represents the mean ± SD from 8 replicates. Different letters above bars denotes a significant difference at P<0.001 using a one-way ANOVA with Dunn's test. **(C)** Splicing ratio of *RB* in *RB* transgenic *N. benthamiana*following agroinfiltration of RNAi-hairpin constructs for 1 day and inoculation with *P. infestans* zoospores. RNA was extracted 2 days after pathogen inoculation. Transcript levels were detected by RT-qPCR and normalized to RB_CDS in RNAi-EV and following mock treatment. Bars represent the mean ± SD in three independent replicates. **(D)** Agroinfiltration of IPI-O1 in *RB* and *RB_CDS* transgenic *N. benthamiana* with DMSO (control), 1μM splicing modulator Pladienolide B (Pla-B), or 30μM Pla-B. Cell death was visually assessed and photographed at 4 dpi (left). Numbers show the ratio of infiltrated areas with cell death compared to the areas showing no cell death. Electrolyte leakage was monitored by conductivity measurements following the same treatments (right). Data represents the mean ± SD from 8 replications. **(E)** Splicing ratio of *RB* in *RB* transgenic *N. benthamiana* following treatment with DMSO (control), 1μM Pla-B, or 30μM Pla-B and inoculation with *P. infestans* zoospores at 2 dpi by RT-qPCR. For all graphs, ns = no significant difference and three asterisks denotes a statistical difference at P<0.001 using a two-way ANOVA with Tukey's test..

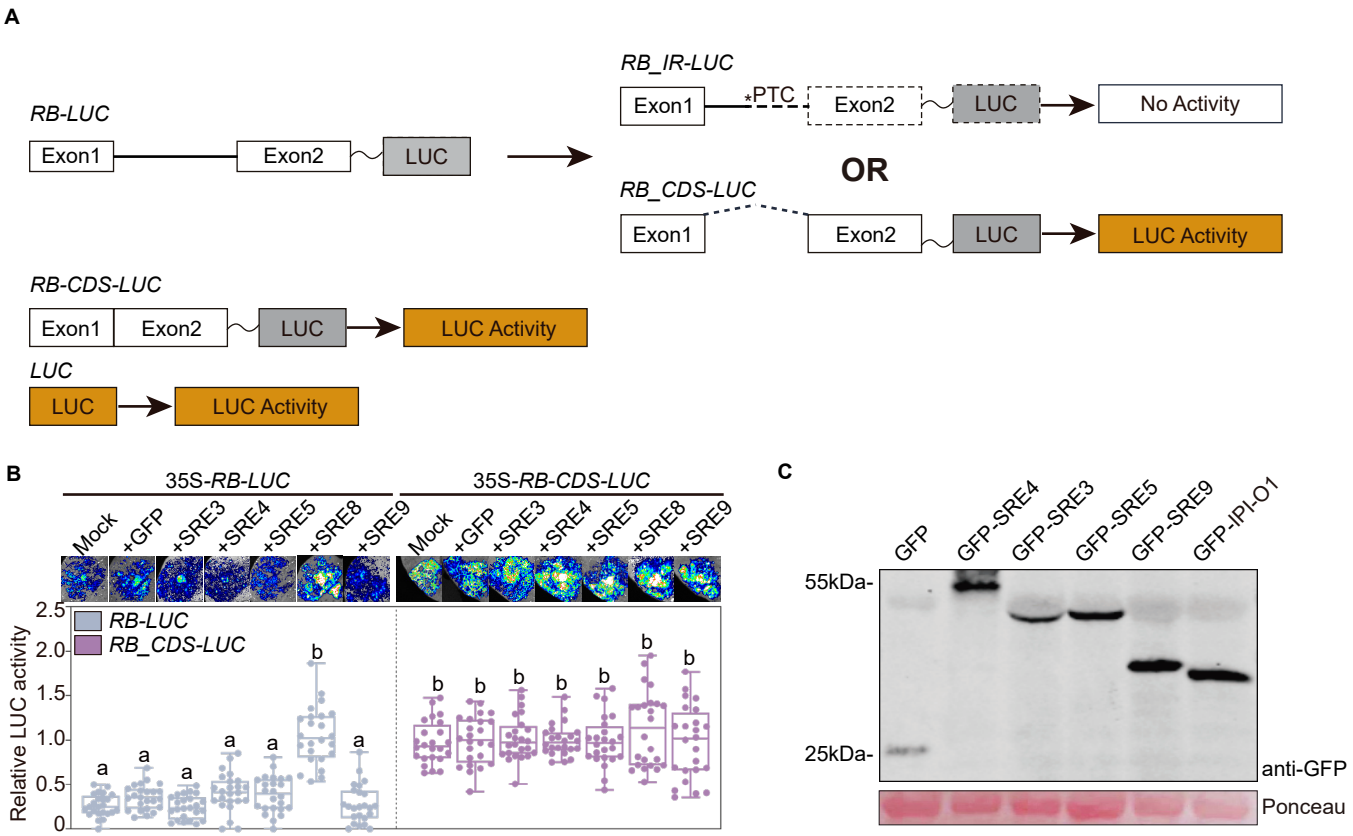

Figure 5. IPI-O1 induces *RB* intron splicing.
(A) Schematic diagram of the *RB_LUC* alternative splicing reporter system. The genomic sequence of *RB* was fused with the *luciferase* (*LUC*) gene to construct 35S::*RB-LUC*. Intron retention introduces a premature termination codon (PTC) and no production of the luciferase reporter. Intron splicing leads to a full-length RB-LUC protein with luciferase activity. The 35S::*RB_CDS-LUC* construct with the intron removed produces a full-length RB-LUC protein with luciferase activity regardless of intron splicing activity. The 35S::*LUC* construct is a positive control. **(B)** Results of co-expression of the reporters with multiple splicing regulatory effectors (SRE; Huang et al., 2020). LUC activity was quantified at 48 hpi. 24 individual leaf discs were collected for LUC activity measurement, and relative LUC activity was normalized to the activity of the 35S::*RB_CDS-LUC* construct with mock treatment. Data represents the mean ± SD from 24 replications. Different letters above each bar represent a significant difference at P<0.001 using a two-way ANOVA with Dunn's test. **(C)** GFP-tagged SRE fusion protein expression in *N. benthamiana* was confirmed by western blotting using an anti-GFP antibody. Protein loading was visualized by Ponceau S staining.

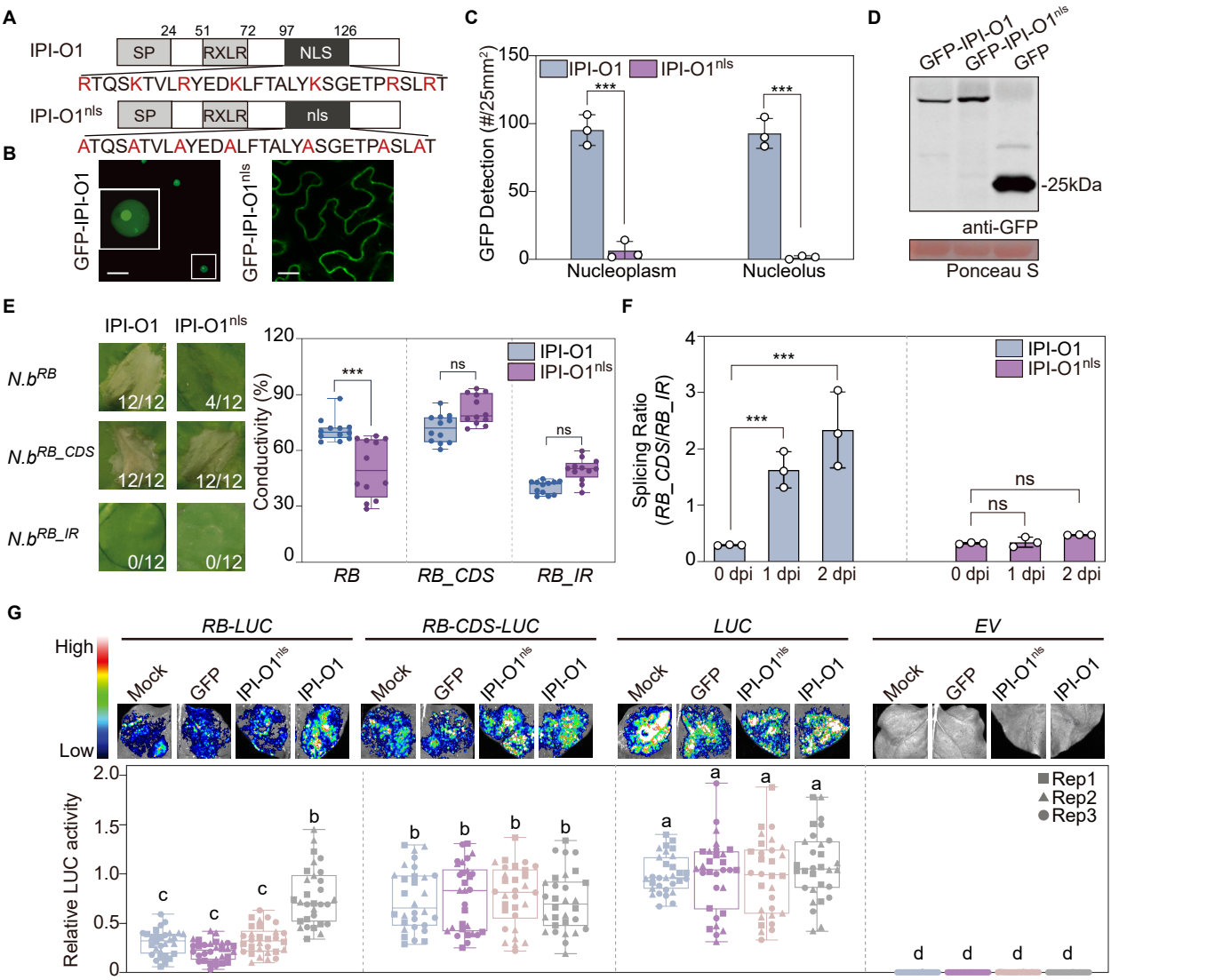

Figure 6. Nuclear localization of IPI-O1 is necessary for *RB* intron splicing.
(A) Schematic diagrams at the top show the location of alanine replacements within the nuclear localization signal of IPI-O1. GFP-IPI-O1 and GFP-IPI-O1^{nls} were expressed in *N. benthamiana* leaves for 48 h before imaging, Scale bar = 20 µm. **(B)** Bars represent the number of times that GFP was detected in the nucleoplasm or nucleolus following infiltration of GFP-IPI-O1 and GFP-IPI-O1^{nls}. Data represents the mean ± SD of three replicates. **(C)** Expression of GFP-tagged fusions of IPI-O1 and IPI-O1^{nls} in *N. benthamiana* was confirmed by western blotting using an anti-GFP antibody. Protein loading was visualized by Ponceau S staining. **(D)** On the left are visual examples and incidence ratios of hypersensitive cell death responses following agroinfiltration of IPI-O1 and IPI-O1^{nls} in leaves of *RB*, *RB_CDS*, and *RB_IR* transgenic *N. benthamiana*. Cell death was visually assessed and photographed at 4 dpi. The right shows results of electrolyte leakage assays of infiltrated areas. Data represents the mean ± SD of 12 replications. **(E)** Splicing ratio of *RB* in *RB* transgenic *N. benthamiana* following agroinfiltration of IPI-O1 and IPI-O1^{nls} at 2 dpi by RT-qPCR. Bars represent the mean ± SD of three independent replicates. **(F)** Results of co-expression of *RB LUC* reporters with mock, GFP, IPI-O1 and IPI-O1^{nls} in *N. benthamiana* leaves by agroinfiltration. LUC activity was quantified at 2 dpi. Relative LUC activity was normalized to the activity of the 35S-LUC construct with mock treatment. Data represents the mean ± SD of 30 replications. For all graphs, ns = no significant difference and three asterisks denotes a statistical difference at P<0.001 using a two-way ANOVA with Tukey's test..

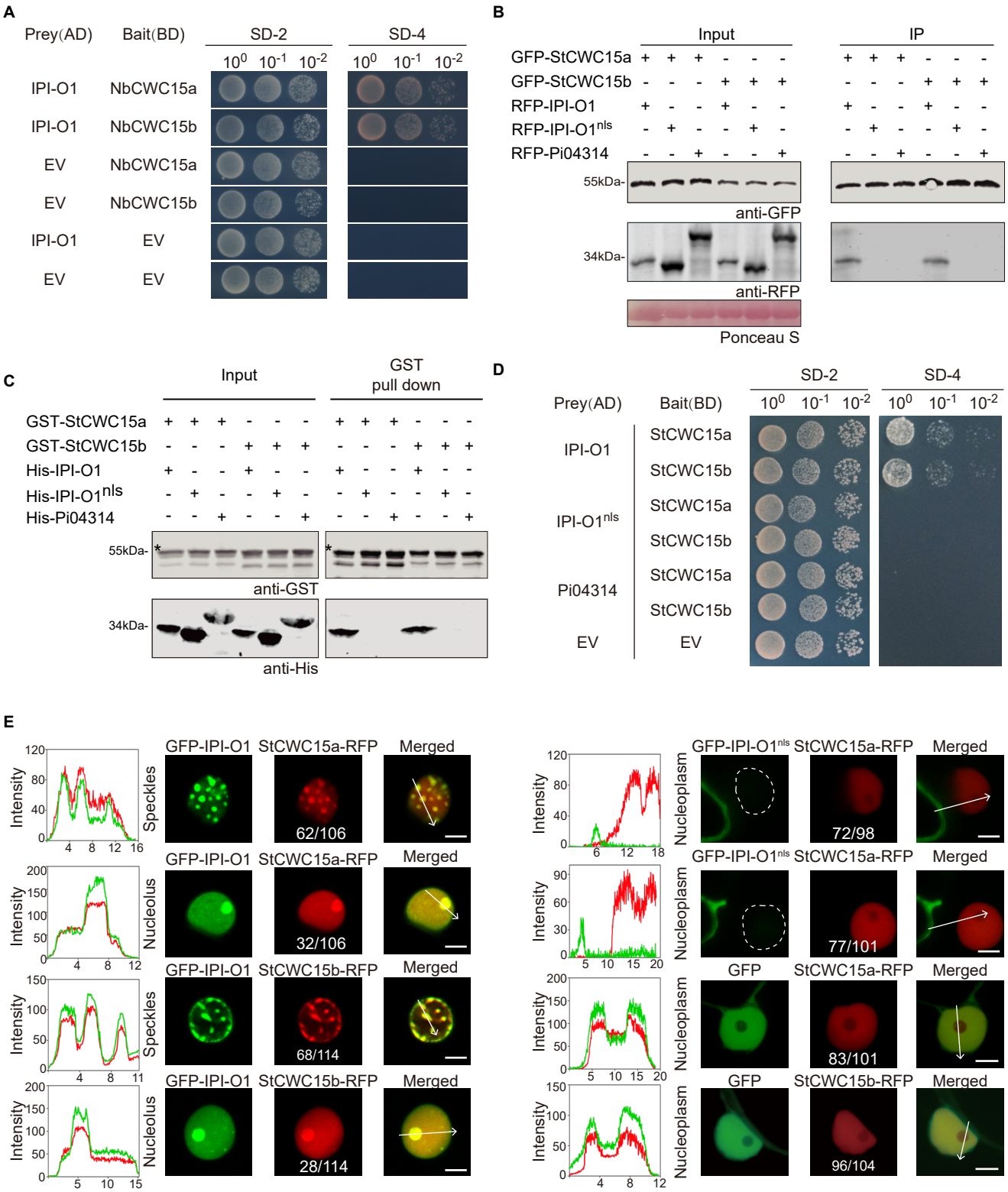

Figure 7. IPI-O1 interacts physically with splicing factor CWC15.
(A) Yeast-two hybrid interaction between IPI-O1, CWC15 variants, and splicing factors from *N. benthamiana*. Yeast transformants were spotted as 10-fold serial dilutions on SD medium without leucine and tryptophan (SD–2), or without histidine, leucine, adenine, and tryptophan (SD–4). Yeast cells were photographed 2-3 days after plating. Empty BD and AD plasmids (EV) were used ascontrols. Experiments were performed at least three times with similar results. **(B)** Silencing of *CWC15* leads to loss of *RB*-mediated HR. IPI-O1 was co-expressed with the indicated RNAi constructs in *RB* transgenic *N. benthamiana*. Numbers represent the incidence ratios of hypersensitive cell death responses. Infiltrated areas were photographed 4 dpi. Electrolyte leakage was monitored by conductivity measurements following the same treatments (bottom). Data represents the mean ± SD from 12 replications. Different letters designate a significant difference from the empty vector (EV) control at $P<0.01$.
(C) Immunoprecipitation (IP) of StCWC15a/b-GFP with RFP-IPI-O1, RFP-IPI-O1^{nls}, or RFP-Pi04314 following agroinfiltration in *N. benthamiana* leaves. Expression of constructs in the leaves is indicated by +. Protein size markers are indicated in kDa, and the Ponceau S stain was used to show levels of protein loading. **(D)** *In vitro* pulldown assay using the GST-tagged StCWC15a/b to immunoprecipitate IPI-O1 and IPI-O1^{nls}. Input

and GST-pulldown proteins were visualized by protein blotting using anti-GST and anti-His antibodies. Asterisks (*) indicate the protein bands that correspond to the expected size of CWC15. **(E)** IPI-O1 co-localizes with StCWC15 in nuclear speckles and the nucleolus. GFP-IPI-O1, GFP-IPI-O1^{nls}, and GFP alone were transiently co-expressed with StCWC15a/b-RFP by agroinfiltration in *N. benthamiana*. The left image is from the GFP channel, the middle image is from the RFP channel, and the right image is the overlay of the GFP and RFP channels. Numbers represent the frequency of cells showing indicated StCWC15 subcellular localization compared to the total StCWC15-positive cells in 25mm^2 discs from three biological replicates. Graphs show the fluorescence intensity profiles across the arrows in the merged images. Bar = 5μm.

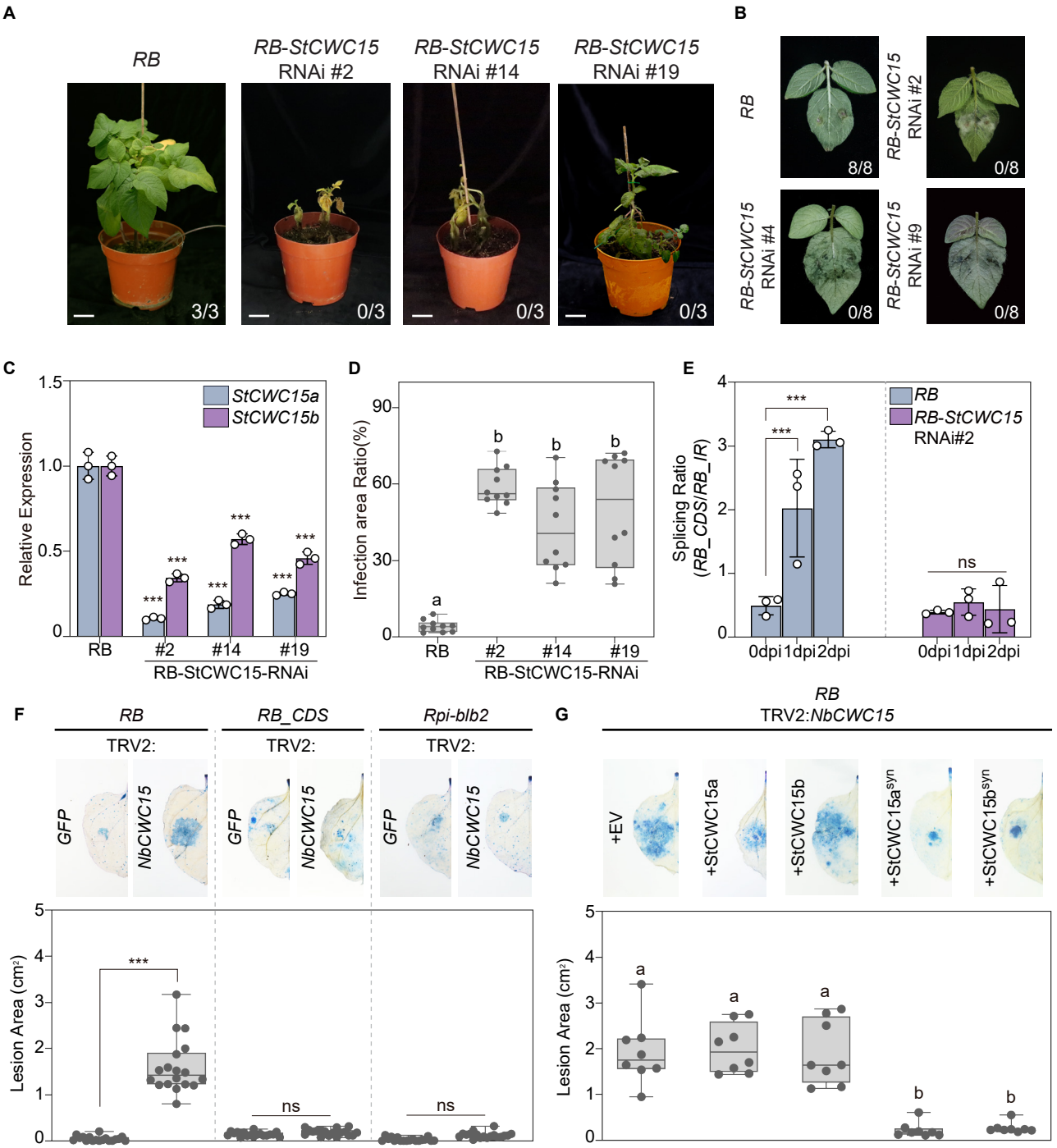

Figure 8. Silencing *StCWC15* disrupts *RB*-mediated resistance.
(A) Whole plants were spray-inoculated (left) and detached leaves were drop-inoculated (right) with zoospores of *P. infestans* strain JH19 in *RB* and *RB-StCWC15* RNAi transgenic potato. Bar = 3 cm. The number represents the frequency of leaves showing resistance compared to all inoculated leaves. **(B)** Relative expression of *StCWC15a/b* in three RNAi transformed lines compared to *RB* transgenic potato. Bars represent the mean ± SD of three independent replicates. Three asterisks designate a statistical difference from the RB control at P<0.01. **(C)** Infection ratio of *P. infestans* JH19 on *RB* and *RB-StCWC15* RNAi transgenic potato lines. Data represents the mean ± SD from 10 repliactions. Different letters denote a significance difference at P<0.001. **(D)** Splicing ratio of *RB* in *RB-StCWC15* RNAi transgenic potato line #2 following inoculation with *P. infestans* zoospores at 2 dpi by RT-qPCR. Bars represent the mean ± SD from three independent replicates. ns=no significant difference and three asterisks denotes a statistical difference at P<0.001. **(F)** *NbCWC15* was silenced by VIGS in *RB*, *RB_CDS*, and *Rpi_blb2* transgenic *N. benthamiana* and inoculated with *P. infestans* JH19 on detached leaves. Photos (top) and lesion areas (bottom) were recorded at 5 dpi. Lesion area data represents the mean ± SD from 18 replications. **(G)** Complementation of *RB* function caused by *CWC15* silencing in *N. benthamiana* via synthetic *StCWC15* constructs (*StCWC15a/b*^{syn}). Agrobacterium expressing *StCWC15a/b*^{syn} constructs were infiltrated into *NbCWC15* silenced *RB* transgenic *N. benthmiana*, then inoculated with *P. infestans* JH19 zoospores. Photos and lesion areas were recorded at 5 dpi. Data represent the mean ± SD from 8 replications. Different letters denote a significance difference at P<0.001 using one-way ANOVA with Dunn's test.

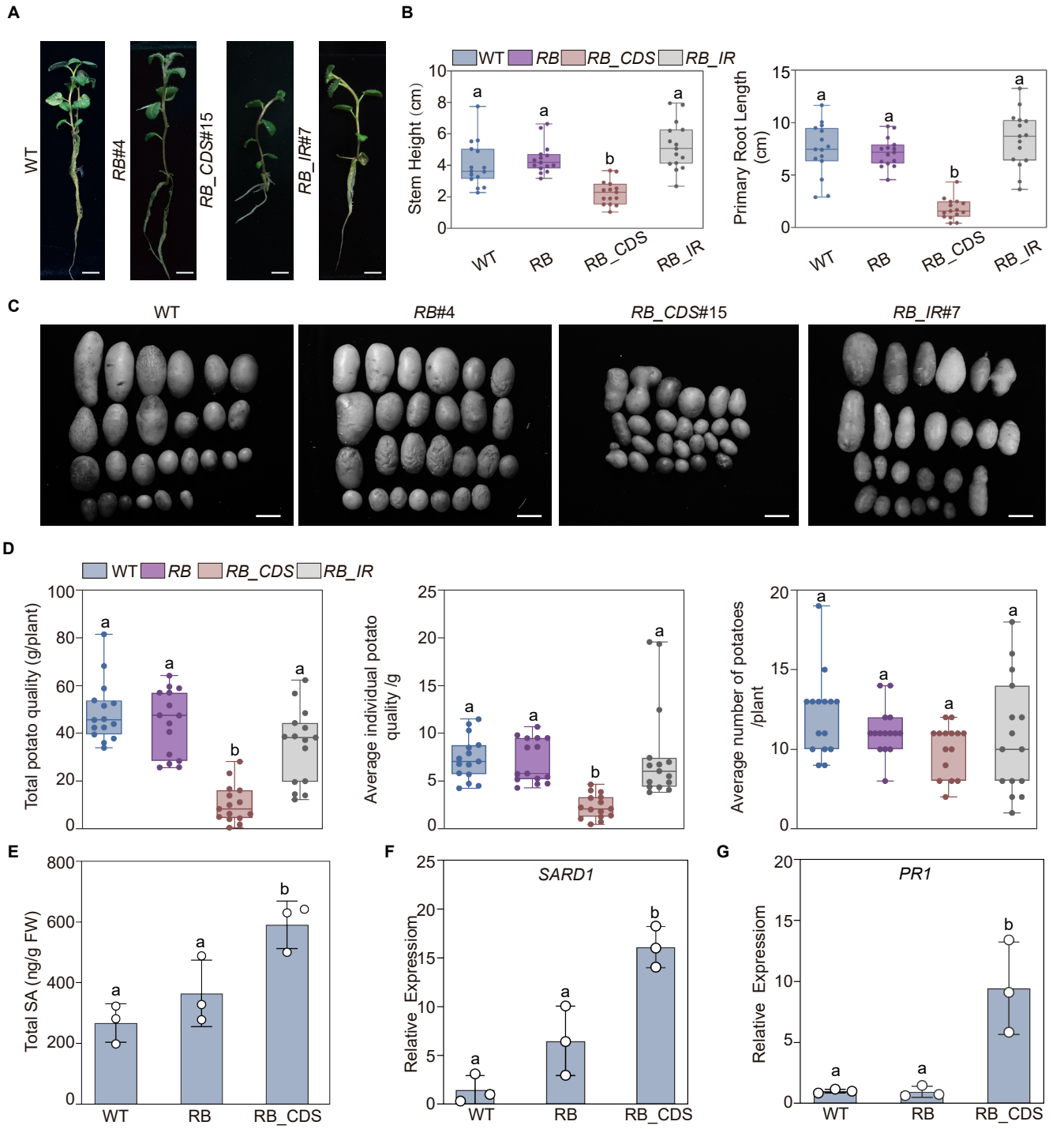

Figure 9. Alternative intron splicing of *RB* balances plant growth and immunity.
(A) Photos of 21-day-old wild-type (WT) Favorita and *RB*, *RB_CDS*, and *RB_IR* transgenic tissue culture plants. Bar = 1 cm. **(B)** Average stem height and root length of Favorita (WT) and 21 day-old transgenic potato tissue culture plants. Bars represent the mean ± SD from 15 tissue culture plants. **(C)** Tubers of Favorita (WT) and transgenic plants. Tubers were harvested and photographed 8 to 10 weeks after tissue culture plants were transplanted. Bar = 1 cm. **(D)** Average tuber yield, average individual tuber mass, and average number of tubers from greenhouse grown plants. Measurements were taken at 8 to 10 weeks after tissue culture plants were transplanted. Bars represent the mean ± SD from 15 replications of 3 independent lines for each genotype. **(E)** Total salicylic acid (SA) content in Favorita (WT) and transgenic *RB* and *RB_CDS* lines without pathogen inoculation. FW, fresh weight. Bars represent the mean ± SD from three independent replicates. **(F-G)** Relative expression of *SARD1* (F) and *PR1* (G) in the indicated transgenic potato as determined by RT-qPCR. Bars represent the mean ± SD from three independent replicates. For all graphs, different letters represent a statistical difference at P<0.001 using one-way ANOVA with Dunn's test.

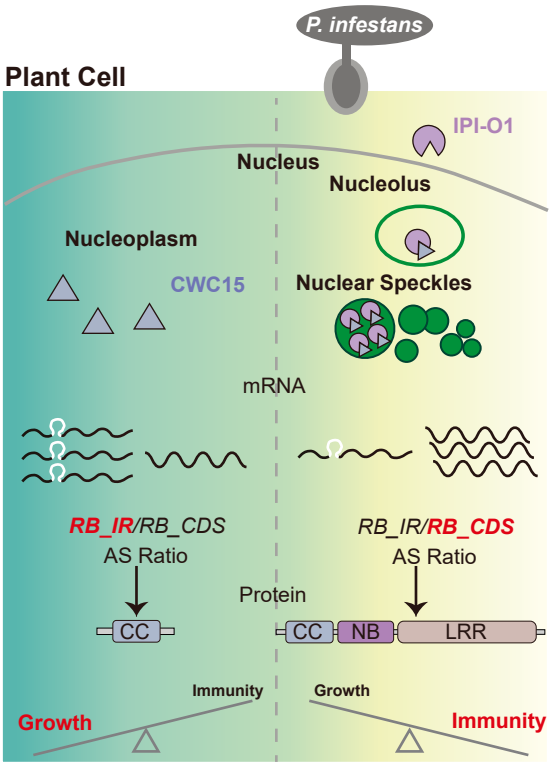

Fig.10 Schematic model of the *P. infestans*-host pathosystem related to resistance gene *RB* and effector IPI-O1.
During normal growth (left), CWC15 proteins (grey triangles) are maintained in the nucleoplasm and *RB* transcripts exist primarily with the intron retained (*RB_IR*). This results in the production of a truncated, non-functional RB protein that supports growth over immunity. Following *P. infestans* infection, effector IPI-O1 is introduced into the plant cell and translocates to the nucleus, leading to a re-localization of CWC15 from the nucleoplasm to the nucleolus and speckles. This results in increased splicing of the RB intron (*RB_CDS)*, resulting in production of a full-length RB protein that can elicit immunity.

Parsed Citations

Axtell, M.J., and Staskawicz, B.J. (2003). Initiation of RPS2-specified disease resistance in Arabidopsis is coupled to the AvrRpt2-directed elimination of RIN4. Cell 112, 369-377.
Google Scholar: Author Only Title Only Author and Title

Barta, A., Kalyna, M., and Lorković, Z.J. (2008). Plant SR Proteins and Their Functions. In Nuclear pre-mRNA Processing in Plants, A.S.N. Reddy and M. Golovkin, eds (Berlin, Heidelberg: Springer Berlin Heidelberg), pp. 83-102.
Google Scholar: Author Only Title Only Author and Title

Bazin, J., Mariappan, K., Jiang, Y., Blein, T., Voelz, R., Crespi, M., and Hirt, H. (2020). Role of MPK4 in pathogen-associated molecular pattern-triggered alternative splicing in Arabidopsis. PLoS Pathog 16, e1008401.
Google Scholar: Author Only Title Only Author and Title

Bhaskar, P.B., Raasch, J.A., Kramer, L.C., Neumann, P., Wielgus, S.M., Austin-Phillips, S., and Jiang, J. (2008). Sgt1, but not Rar1, is essential for the RB-mediated broad-spectrum resistance to potato late blight. BMC Plant Biol 8, 8.
Google Scholar: Author Only Title Only Author and Title

Boevink, P.C., Wang, X., McLellan, H., He, Q., Naqvi, S., Armstrong, M.R., Zhang, W., Hein, I., Gilroy, E.M., and Tian, Z. (2016). A Phytophthora infestans RXLR effector targets plant PP1c isoforms that promote late blight disease. Nature Communications 7, 10311.
Google Scholar: Author Only Title Only Author and Title

Bradeen, J.M., Iorizzo, M., Mollov, D.S., Raasch, J., Kramer, L.C., Millett, B.P., Austin-Phillips, S., Jiang, J., and Carputo, D. (2009). Higher copy numbers of the potato RB transgene correspond to enhanced transcript and late blight resistance levels. Molecular Plant-Microbe Interactions 22, 437-446.
Google Scholar: Author Only Title Only Author and Title

Cesari, S., Bernoux, M., Moncuquet, P., Kroj, T., and Dodds, P.N. (2014). A novel conserved mechanism for plant NLR protein pairs: the "integrated decoy" hypothesis. Front Plant Sci 5, 606.
Google Scholar: Author Only Title Only Author and Title

Champouret, N., Bouwmeester, K., Rietman, H., Lee, T.v.d., Maliepaard, C., Heupink, A., Vondervoort, P.J.I.v.d., Jacobsen, E., Visser, R.G.F., Vossen, E.A.G.v.d., Govers, F., and Vleeshouwers, V.G.A.A. (2009). Phytophthora infestans Isolates Lacking Class I ipiO Variants Are Virulent on Rpi-blb1 Potato. MPMI 22, 1535-1545.
Google Scholar: Author Only Title Only Author and Title

Chen, M., and Manley, J.L. (2009). Mechanisms of alternative splicing regulation: insights from molecular and genomics approaches. Nat Rev Mol Cell Biol 10, 741-754.
Google Scholar: Author Only Title Only Author and Title

Chen, Y., Liu, Z., and Halterman, D.A. (2012). Molecular determinants of resistance activation and suppression by Phytophthora infestans effector IPI-O. PLoS Pathogen 8, e1002595.
Google Scholar: Author Only Title Only Author and Title

Cheng, Y.T., Li, Y., Huang, S., Huang, Y., Dong, X., Zhang, Y., and Li, X. (2011). Stability of plant immune-receptor resistance proteins is controlled by SKP1-CULLIN1-F-box (SCF)-mediated protein degradation. Proc Natl Acad Sci U S A 108, 14694-14699.
Google Scholar: Author Only Title Only Author and Title

Couto, D., and Zipfel, C. (2016). Regulation of pattern recognition receptor signalling in plants. Nat Rev Immunol 16, 537-552.
Google Scholar: Author Only Title Only Author and Title

Cretu, C., Agrawal, A.A., Cook, A., Will, C.L., Fekkes, P., Smith, P.G., Luhrmann, R., Larsen, N., Buonamici, S., and Pena, V. (2018). Structural Basis of Splicing Modulation by Antitumor Macrolide Compounds. Mol Cell 70, 265-273 e268.
Google Scholar: Author Only Title Only Author and Title

Cui, C., Wang, J.-J., Zhao, J.-H., Fang, Y.-Y., He, X.-F., Guo, H.-S., and Duan, C.-G. (2020). A Brassica miRNA Regulates Plant Growth and Immunity through Distinct Modes of Action. Mol. Plant 13, 231-245.
Google Scholar: Author Only Title Only Author and Title

Cui, H., Tsuda, K., and Parker, J.E. (2015). Effector-Triggered Immunity: From Pathogen Perception to Robust Defense. Annual Review of Plant Biology 66, 487-511.
Google Scholar: Author Only Title Only Author and Title

Dagdas, Y.F., Belhaj, K., Maqbool, A., Chaparro-Garcia, A., Pandey, P., Petre, B., Tabassum, N., Cruz-Mireles, N., Hughes, R.K., Sklenar, J., Win, J., Menke, F., Findlay, K., Banfield, M.J., Kamoun, S., and Bozkurt, T.O. (2016). An effector of the Irish potato famine pathogen antagonizes a host autophagy cargo receptor. Elife 5.
Google Scholar: Author Only Title Only Author and Title

Dangl, J.L., and Jones, J.D.G. (2001). Plant pathogens and integrated defence responses to infection. Nature 411, 826-833.

Google Scholar: Author Only Title Only Author and Title

Deng, Y., Zhai, K., Xie, Z., Yang, D., Zhu, X., Liu, J., Wang, X., Qin, P., Yang, Y., Zhang, G., Li, Q., Zhang, J., Wu, S., Milazzo, J., Mao, B., Wang, E., Xie, H., Tharreau, D., and He, Z. (2019). Epigenetic regulation of antagonistic receptors confers rice blast resistance with yield balance. Science 355, 962-965.
Google Scholar: Author Only Title Only Author and Title

Dinesh-Kumar, S.P., and Baker, B.J. (2000). Alternatively spliced N resistance gene transcripts: Their possible role in tobacco mosaic virus resistance. Proc. Natl Acad. Sci. USA 97, 1908–1913.
Google Scholar: Author Only Title Only Author and Title

Dinh, H.X., Singh, D., Gomez de la Cruz, D., Hensel, G., Kumlehn, J., Mascher, M., Stein, N., Perovic, D., Ayliffe, M., Moscou, M.J., Park, R.F., and Pourkheirandish, M. (2022). The barley leaf rust resistance gene Rph3 encodes a predicted membrane protein and is induced upon infection by avirulent pathotypes of Puccinia hordei. Nature Communications 13, 2386.
Google Scholar: Author Only Title Only Author and Title

Dodds, P.N., and Rathjen, J.P. (2010). Plant immunity: towards an integrated view of plant-pathogen interactions. Nature reviews. Genetics 11, 539-548.
Google Scholar: Author Only Title Only Author and Title

Dodds, P.N., Lawrence, G.J., Catanzariti, A.-M., Teh, T., Wang, C.-I.A., Ayliffe, M.A., Kobe, B., and Ellis, J.G. (2006). Direct protein interaction underlies gene-for-gene specificity and coevolution of the flax resistance genes and flax rust avirulence genes. Proceedings of the National Academy of Sciences 103, 8888-8893.
Google Scholar: Author Only Title Only Author and Title

Duxbury, Z., Wu, C.H., and Ding, P. (2021). A Comparative Overview of the Intracellular Guardians of Plants and Animals: NLRs in Innate Immunity and Beyond. Annu Rev Plant Biol 72, 155-184.
Google Scholar: Author Only Title Only Author and Title

Filichkin, S.A., Priest, H.D., Givan, S.A., Shen, R., Bryant, D.W., Fox, S.E., Wong, W.-K., and Mockler, T.C. (2010). Genome-wide mapping of alternative splicing in Arabidopsis thaliana. Genome Research 20, 45-58.
Google Scholar: Author Only Title Only Author and Title

Gao, M., He, Y., Yin, X., Zhong, X., Yan, B., Wu, Y., Chen, J., Li, X., Zhai, K., Huang, Y., Gong, X., Chang, H., Xie, S., Liu, J., Yue, J., Xu, J., Zhang, G., Deng, Y., Wang, E., Tharreau, D., Wang, G.L., Yang, W., and He, Z. (2021a). Ca(2+) sensor-mediated ROS scavenging suppresses rice immunity and is exploited by a fungal effector. Cell 184, 5391-5404 e5317.
Google Scholar: Author Only Title Only Author and Title

Gao, W., Liu, Y., Huang, J., Chen, Y., Chen, C., Lu, L., Zhao, H., Men, S., and Zhang, X. (2021b). MES7 Modulates Seed Germination via Regulating Salicylic Acid Content in Arabidopsis. Plants (Basel) 10.
Google Scholar: Author Only Title Only Author and Title

Halterman, D., Wei, F., and Wise, R. (2003). Powdery mildew induced Mla mRNAs are alternatively spliced and contain multiple upstream open reading frames. Plant Physiol 131, 558-567.
Google Scholar: Author Only Title Only Author and Title

Halterman, D.A., and Wise, R.P. (2006). Upstream open reading frames of the barley Mla13 powdery mildew resistance gene function co-operatively to down-regulate translation. Molecular Plant Pathology 7, 167-176.
Google Scholar: Author Only Title Only Author and Title

Haverkort, A.J., Struik, P.C., Visser, R.G.F., and Jacobsen, E. (2009). Applied Biotechnology to Combat Late Blight in Potato Caused by Phytophthora Infestans. Potato Research 52, 249-264.
Google Scholar: Author Only Title Only Author and Title

He, Z., Webster, S., and He, S.Y. (2022). Growth-defense trade-offs in plants. Current Biology 32, R634-R639.
Google Scholar: Author Only Title Only Author and Title

Huang, C.Y., Rangel, D.S., Qin, X., Bui, C., Li, R., Jia, Z., Cui, X., and Jin, H. (2021). The chromatin-remodeling protein BAF60/SWP73A regulates the plant immune receptor NLRs. Cell Host Microbe 29, 425-434 e424.
Google Scholar: Author Only Title Only Author and Title

Huang, J., Lu, X., Wu, H., Xie, Y., Peng, Q., Gu, L., Wu, J., Wang, Y., Reddy, A.S.N., and Dong, S. (2020). Phytophthora effectors modulate genome-wide alternative splicing of host mRNAs to reprogram plant immunity. Molecular plant 13, 1470-1484.
Google Scholar: Author Only Title Only Author and Title

Huang, J., Gu, L., Zhang, Y., Yan, T., Kong, G., Kong, L., Guo, B., Qiu, M., Wang, Y., Jing, M., Xing, W., Ye, W., Wu, Z., Zhang, Z., Zheng, X., Gijzen, M., Wang, Y., and Dong, S. (2017). An oomycete plant pathogen reprograms host pre-mRNA splicing to subvert immunity. Nature Communications 8.
Google Scholar: Author Only Title Only Author and Title

Jia, J., Long, Y., Zhang, H., Li, Z., Liu, Z., Zhao, Y., Lu, D., Jin, X., Deng, X., Xia, R., Cao, X., and Zhai, J. (2020). Post-transcriptional

splicing of nascent RNA contributes to widespread intron retention in plants. Nature Plants 6, 780-788.
Google Scholar: Author Only Title Only Author and Title

Jones, J.D., and Dangl, J.L. (2006). The plant immune system. Nature 444, 323-329.
Google Scholar: Author Only Title Only Author and Title

Jung, H.W., Panigrahi, G.K., Jung, G.Y., Lee, Y.J., Shin, K.H., Sahoo, A., Choi, E.S., Lee, E., Man Kim, K., Yang, S.H., Jeon, J.S., Lee, S.C., and Kim, S.H. (2020). Pathogen-associated molecular pattern-triggered immunity involves proteolytic degradation of core nonsense-mediated mRNA decay factors during the early defense response. Plant Cell 32, 1081-1101.
Google Scholar: Author Only Title Only Author and Title

Kamoun, S., and Smart, C.D. (2005). Late Blight of Potato and Tomato in the Genomics Era. Plant Disease 89, 692-699.
Google Scholar: Author Only Title Only Author and Title

Kamoun, S., Furzer, O., Jones, J.D.G., Judelson, H.S., Ali, G.S., Dalio, R.J.D., Roy, S.G., Schena, L., Zambounis, A., Panabieres, F., Cahill, D., Ruocco, M., Figueiredo, A., Chen, X.R., Hulvey, J., Stam, R., Lamour, K., Gijzen, M., Tyler, B.M., Grunwald, N.J., Mukhtar, M.S., Tome, D.F.A., Tor, M., Van den Ackerveken, G., McDowell, J., Daayf, F., Fry, W.E., Lindqvist-Kreuze, H., Meijer, H.J.G., Petre, B., Ristaino, J., Yoshida, K., Birch, P.R.J., and Govers, F. (2015). The Top 10 oomycete pathogens in molecular plant pathology. Molecular Plant Pathology 16, 413-434.
Google Scholar: Author Only Title Only Author and Title

Karki, H.S., Jansky, S.H., and Halterman, D.A. (2021). Screening of Wild Potatoes Identifies New Sources of Late Blight Resistance. Plant Disease 105, 368-376.
Google Scholar: Author Only Title Only Author and Title

Katou, S., Yoshioka, H., Kawakita, K., Rowland, O., Jones, J.D.G., Mori, H., and Doke, N. (2005). Involvement of PPS3 Phosphorylated by Elicitor-Responsive Mitogen-Activated Protein Kinases in the Regulation of Plant Cell Death. Plant Physiology 139, 1914-1926.
Google Scholar: Author Only Title Only Author and Title

Klepikova, A.V., Kasianov, A.S., Gerasimov, E.S., Logacheva, M.D., and Penin, A.A. (2016). A high resolution map of the Arabidopsis thaliana developmental transcriptome based on RNA-seq profiling. The Plant Journal 88, 1058-1070.
Google Scholar: Author Only Title Only Author and Title

Kotake, Y., Sagane, K., Owa, T., Mimori-Kiyosue, Y., Shimizu, H., Uesugi, M., Ishihama, Y., Iwata, M., and Mizui, Y. (2007). Splicing factor SF3b as a target of the antitumor natural product pladienolide. Nat Chem Biol 3, 570-575.
Google Scholar: Author Only Title Only Author and Title

Lai, Y., and Eulgem, T. (2018). Transcript-level expression control of plant NLR genes. Mol Plant Pathol 19, 1267-1281.
Google Scholar: Author Only Title Only Author and Title

Li, F., Pignatta, D., Bendix, C., Brunkard, J.O., Cohn, M.M., Tung, J., Sun, H., Kumar, P., and Baker, B. (2012). MicroRNA regulation of plant innate immune receptors. Proceedings of the National Academy of Sciences USA 109, 1790-1795.
Google Scholar: Author Only Title Only Author and Title

Li, X., Kapos, P., and Zhang, Y. (2015). NLRs in plants. Curr Opin Immunol 32, 114-121.
Google Scholar: Author Only Title Only Author and Title

Liao, S.E., and Regev, O. (2021). Splicing at the phase-separated nuclear speckle interface: a model. Nucleic Acids Res 49, 636-645.
Google Scholar: Author Only Title Only Author and Title

Liu, N., Hake, K., Wang, W., Zhao, T., Romeis, T., and Tang, D. (2017). CALCIUM-DEPENDENT PROTEIN KINASE5 Associates with the Truncated NLR Protein TIR-NBS2 to Contribute to exo70B1-Mediated Immunity. Plant Cell 29, 746-759.
Google Scholar: Author Only Title Only Author and Title

Long, Jennifer C., and Caceres, Javier F. (2008). The SR protein family of splicing factors: master regulators of gene expression. Biochemical Journal 417, 15-27.
Google Scholar: Author Only Title Only Author and Title

Lu, Q., Tang, X., Tian, G., Wang, F., Liu, K., Nguyen, V., Kohalmi, S.E., Keller, W.A., Tsang, E.W.T., Harada, J.J., Rothstein, S.J., and Cui, Y. (2010a). Arabidopsis homolog of the yeast TREX-2 mRNA export complex: components and anchoring nucleoporin. The Plant Journal 61, 259-270.
Google Scholar: Author Only Title Only Author and Title

Lu, T., Lu, G., Fan, D., Zhu, C., Li, W., Zhao, Q., Feng, Q., Zhao, Y., Guo, Y., Li, W., Huang, X., and Han, B. (2010b). Function annotation of the rice transcriptome at single-nucleotide resolution by RNA-seq. Genome Research 20, 1238-1249.
Google Scholar: Author Only Title Only Author and Title

Maqbool, A., Saitoh, H., Franceschetti, M., Stevenson, C.E., Uemura, A., Kanzaki, H., Kamoun, S., Terauchi, R., and Banfield, M.J.

(2015). Structural basis of pathogen recognition by an integrated HMA domain in a plant NLR immune receptor. Elife 4.
Google Scholar: Author Only Title Only Author and Title

Marquez, Y., Brown, J.W.S., Simpson, C., Barta, A., and Kalyna, M. (2012). Transcriptome survey reveals increased complexity of the alternative splicing landscape in Arabidopsis. Genome Research 22, 1184-1195.
Google Scholar: Author Only Title Only Author and Title

Ning, Y., Liu, W., and Wang, G.L. (2017). Balancing Immunity and Yield in Crop Plants. Trends Plant Sci 22, 1069-1079.
Google Scholar: Author Only Title Only Author and Title

Nishimura, M.T., Anderson, R.G., Cherkis, K.A., Law, T.F., Liu, Q.L., Machius, M., Nimchuk, Z.L., Yang, L., Chung, E.H., El Kasmi, F., Hyunh, M., Osborne Nishimura, E., Sondek, J.E., and Dangl, J.L. (2017). TIR-only protein RBA1 recognizes a pathogen effector to regulate cell death in Arabidopsis. Proceedings of the National Academy of Sciences USA 114, E2053-E2062.
Google Scholar: Author Only Title Only Author and Title

Ofir, G., Herbst, E., Baroz, M., Cohen, D., Millman, A., Doron, S., Tal, N., Malheiro, D.B.A., Malitsky, S., Amitai, G., and Sorek, R. (2021). Antiviral activity of bacterial TIR domains via immune signalling molecules. Nature 600, 116-120.
Google Scholar: Author Only Title Only Author and Title

Palma, K., Zhao, Q., Cheng, Y.T., Bi, D., Monaghan, J., Cheng, W., Zhang, Y., and Li, X. (2007). Regulation of plant innate immunity by three proteins in a complex conserved across the plant and animal kingdoms. Genes & Development 21, 1484-1493.
Google Scholar: Author Only Title Only Author and Title

Paluchowska, P., Sliwka, J., and Yin, Z. (2022). Late blight resistance genes in potato breeding. Planta 255, 127.
Google Scholar: Author Only Title Only Author and Title

Reddy, A.S. (2007). Alternative splicing of pre-messenger RNAs in plants in the genomic era. Annu Rev Plant Biol 58, 267-294.
Google Scholar: Author Only Title Only Author and Title

Reddy, A.S.N. (2004). Plant serine/arginine-rich proteins and their role in pre-mRNA splicing. Trends in Plant Science 9, 541-547.
Google Scholar: Author Only Title Only Author and Title

Reddy, A.S.N., Marquez, Y., Kalyna, M., and Barta, A. (2013a). Complexity of the Alternative Splicing Landscape in Plants. The Plant Cell 25, 3657-3683.
Google Scholar: Author Only Title Only Author and Title

Reddy, A.S.N., Marquez, Y., Kalyna, M., and Barta, A. (2013b). Complexity of the Alternative Splicing Landscape in Plants The Plant Cell 25, 3657-3683.
Google Scholar: Author Only Title Only Author and Title

Reddy, A.S.N., Huang, J., Syed, N.H., Ben-Hur, A., Dong, S., and Gu, L. (2020). Decoding co-/post-transcriptional complexities of plant transcriptomes and epitranscriptome using next-generation sequencing technologies. Biochemical Society Transactions 48, 2399-2414.
Google Scholar: Author Only Title Only Author and Title

Sanchez-Martin, J., Widrig, V., Herren, G., Wicker, T., Zbinden, H., Gronnier, J., Sporri, L., Praz, C.R., Heuberger, M., Kolodziej, M.C., Isaksson, J., Steuernagel, B., Karafiatova, M., Dolezel, J., Zipfel, C., and Keller, B. (2021). Wheat Pm4 resistance to powdery mildew is controlled by alternative splice variants encoding chimeric proteins. Nat Plants 7, 327-341.
Google Scholar: Author Only Title Only Author and Title

Sarris, P.F., Duxbury, Z., Huh, S.U., Ma, Y., Segonzac, C., Sklenar, J., Derbyshire, P., Cevik, V., Rallapalli, G., Saucet, S.B., Wirthmueller, L., Menke, F.L.H., Sohn, K.H., and Jones, J.D.G. (2015). A Plant Immune Receptor Detects Pathogen Effectors that Target WRKY Transcription Factors. Cell 161, 1089-1100.
Google Scholar: Author Only Title Only Author and Title

Sheth, N., Roca, X., Hastings, M.L., Roeder, T., Krainer, A.R., and Sachidanandam, R. (2006). Comprehensive splice-site analysis using comparative genomics. Nucleic Acids Res 34, 3955-3967.
Google Scholar: Author Only Title Only Author and Title

Slane, D., Lee, C.H., Kolb, M., Dent, C., Miao, Y., Franz-Wachtel, M., Lau, S., Macek, B., Balasubramanian, S., Bayer, M., and Jurgens, G. (2020). The integral spliceosomal component CWC15 is required for development in Arabidopsis. Sci Rep 10, 13336.
Google Scholar: Author Only Title Only Author and Title

Song, J., Bradeen, J.M., Naess, S.K., Raasch, J.A., Wielgus, S.M., Haberlach, G.T., Liu, J., Kuang, H., Austin-Phillips, S., Buell, C.R., Helgeson, J.P., and Jiang, J. (2003). Gene RB cloned from Solanum bulbocastanum confers broad spectrum resistance to potato late blight. Proc Natl Acad Sci U S A 100, 9128-9133.
Google Scholar: Author Only Title Only Author and Title

Stam, M., Mol, J.N.M., and Kooter, J.M. (1997). The silence of genes in transgenic plants. Annals of Botany 79, 3-12.
Google Scholar: Author Only Title Only Author and Title

Sukarta, O.C.A., Zheng, Q., Slootweg, E.J., Mekken, M., Mendel, M., Putker, V., Bertran, A., Brand, A., Overmars, H., Pomp, R., Roosien, J., Boeren, S., Smant, G., and Goverse, A. (2022). GLYCINE-RICH RNA-BINDING PROTEIN 7 potentiates effector-triggered immunity through an RNA recognition motif. Plant Physiol 189, 972-987.
Google Scholar: Author Only Title Only Author and Title

Sun, H., Jiao, W.B., Krause, K., Campoy, J.A., Goel, M., Folz-Donahue, K., Kukat, C., Huettel, B., and Schneeberger, K. (2022). Chromosome-scale and haplotype-resolved genome assembly of a tetraploid potato cultivar. Nat Genet 54, 342-348.
Google Scholar: Author Only Title Only Author and Title

Tsuchiya, T., and Eulgem, T. (2013). An alternative polyadenylation mechanism coopted to the Arabidopsis RPP7 gene through intronic retrotransposon domestication. Proceedings of the National Academy of Sciences USA 110, E3535-3543.
Google Scholar: Author Only Title Only Author and Title

Van de Weyer, A.L., Monteiro, F., Furzer, O.J., Nishimura, M.T., Cevik, V., Witek, K., Jones, J.D.G., Dangl, J.L., Weigel, D., and Bemm, F. (2019). A Species-Wide Inventory of NLR Genes and Alleles in Arabidopsis thaliana. Cell 178, 1260-1272 e1214.
Google Scholar: Author Only Title Only Author and Title

van der Hoorn, R.A., and Kamoun, S. (2008). From Guard to Decoy: a new model for perception of plant pathogen effectors. Plant Cell 20, 2009-2017.
Google Scholar: Author Only Title Only Author and Title

van der Vossen, E., Sikkema, A., Hekkert, B., Gros, J., Stevens, P., Muskens, M., Wouters, D., Pereira, A., Stiekema, W., and Allefs, S. (2003). An ancient R gene from the wild potato species Solanum bulbocastanum confers broad-spectrum resistance to Phytophthora infestans in cultivated potato and tomato. Plant J 36, 867-882.
Google Scholar: Author Only Title Only Author and Title

Vleeshouwers, V.G., Rietman, H., Krenek, P., Champouret, N., Young, C., Oh, S.K., Wang, M., Bouwmeester, K., Vosman, B., Visser, R.G., Jacobsen, E., Govers, F., Kamoun, S., and Van der Vossen, E.A. (2008). Effector genomics accelerates discovery and functional profiling of potato disease resistance and phytophthora infestans avirulence genes. PLoS One 3, e2875.
Google Scholar: Author Only Title Only Author and Title

Wan, R., Bai, R., Zhan, X., and Shi, Y. (2020). How Is Precursor Messenger RNA Spliced by the Spliceosome? Annu Rev Biochem 89, 333-358.
Google Scholar: Author Only Title Only Author and Title

Wang, G., Roux, B., Feng, F., Guy, E., Li, L., Li, N., Zhang, X., Lautier, M., Jardinaud, M.F., Chabannes, M., Arlat, M., Chen, S., He, C., Noel, L.D., and Zhou, J.M. (2015). The Decoy Substrate of a Pathogen Effector and a Pseudokinase Specify Pathogen-Induced Modified-Self Recognition and Immunity in Plants. Cell Host Microbe 18, 285-295.
Google Scholar: Author Only Title Only Author and Title

Wang, J., Hu, M., Wang, J., Qi, J., Han, Z., Wang, G., Qi, Y., Wang, H.W., Zhou, J.M., and Chai, J. (2019). Reconstitution and structure of a plant NLR resistosome conferring immunity. Science 364.
Google Scholar: Author Only Title Only Author and Title

Wang, L., Yang, T., Wang, B., Lin, Q., and Yu, F. (2020). RALF1-FERONIA complex affects splicing dynamics to modulate stress responses and growth in plants. Science Advances 6, eaaz1622.
Google Scholar: Author Only Title Only Author and Title

Wang, S., McLellan, H., Bukharova, T., He, Q., Murphy, F., Shi, J., Sun, S., van Weymers, P., Ren, Y., Thilliez, G., Wang, H., Chen, X., Engelhardt, S., Vleeshouwers, V., Gilroy, E.M., Whisson, S.C., Hein, I., Wang, X., Tian, Z., Birch, P.R.J., and Boevink, P.C. (2018). Phytophthora infestans RXLR effectors act in concert at diverse subcellular locations to enhance host colonization. Journal of Experimental Botany 70, 343-356.
Google Scholar: Author Only Title Only Author and Title

Wu, Z., Zhu, D., Lin, X., Miao, J., Gu, L., Deng, X., Yang, Q., Sun, K., Zhu, D., Cao, X., Tsuge, T., Dean, C., Aoyama, T., Gu, H., and Qu, L.J. (2016). RNA Binding Proteins RZ-1B and RZ-1C Play Critical Roles in Regulating Pre-mRNA Splicing and Gene Expression during Development in Arabidopsis. Plant Cell 28, 55-73.
Google Scholar: Author Only Title Only Author and Title

Xu, F., Xu, S., Wiermer, M., Zhang, Y., and Li, X. (2012). The cyclin L homolog MOS12 and the MOS4-associated complex are required for the proper splicing of plant resistance genes. The plant jouranl 70, 916-928.
Google Scholar: Author Only Title Only Author and Title

Xu, S., Zhang, Z., Jing, B., Gannon, P., Ding, J., Xu, F., Li, X., and Zhang, Y. (2011). Transportin-SR is required for proper splicing of resistance genes and plant immunity. PLOS Genetics 7, e1002159.
Google Scholar: Author Only Title Only Author and Title

Yang, S., Tang, F., and Zhu, H. (2014). Alternative splicing in plant immunity. International journal of molecular sciences 15, 10424-10445.
Google Scholar: Author Only Title Only Author and Title

Zhang, F., Fang, H., Wang, M., He, F., Tao, H., Wang, R., Long, J., Wang, J., Wang, G.L., and Ning, Y. (2022). APIP5 functions as a transcription factor and an RNA-binding protein to modulate cell death and immunity in rice. Nucleic Acids Res 50, 5064-5079.
Google Scholar: Author Only Title Only Author and Title

Zhang, X.-C., and Gassmann, W. (2007). Alternative splicing and mRNA levels of the disease resistance gene RPS4 are induced during defense responses. Plant Physiology 145, 1577-1587.
Google Scholar: Author Only Title Only Author and Title

Zhang, Y., and Li, X. (2005). A putative nucleoporin 96 is required for both basal defense and constitutive resistance responses mediated by suppressor of npr1-1, constitutive 1. The Plant Cell 17, 1306-1316.
Google Scholar: Author Only Title Only Author and Title

Zhang, Y., Xu, S., Ding, P., Wang, D., Cheng, Y.T., He, J., Gao, M., Xu, F., Li, Y., Zhu, Z., Li, X., and Zhang, Y. (2010). Control of salicylic acid synthesis and systemic acquired resistance by two members of a plant-specific family of transcription factors. Proc Natl Acad Sci U S A 107, 18220-18225.
Google Scholar: Author Only Title Only Author and Title

Zhao, J., and Song, J. (2021). NLR immune receptor RB is differentially targeted by two homologous but functionally distinct effector proteins. Plant Communications 2.
Google Scholar: Author Only Title Only Author and Title

Zhou, J.-M., and Chai, J. (2008). Plant pathogenic bacterial type III effectors subdue host responses. Current Opinion in Microbiology 11, 179-185.
Google Scholar: Author Only Title Only Author and Title